Journal of Optimization Theory and Applications
https://doi.org/10.1007/s10957-023-02287-0

Tensor Factorization-Based Method for Tensor Completion with Spatio-temporal Characterization

Quan Yu[1] · **Xinzhen Zhang**[2] · **Zheng-Hai Huang**[2]

Received: 19 August 2021 / Accepted: 9 August 2023

Abstract

In this paper, we propose a novel tensor factorization-based method for the third-order tensor completion problem with spatio-temporal characterization. For this aim, we consider tensor fibered rank, which extends tubal rank, to improve the flexibility and accuracy of data characterization. Based on this rank, we apply a factorization-based method to complete the third-order low-rank tensors with spatio-temporal characteristics, which are intrinsic features of image, video and internet traffic tensor data. The model not only makes good use of the low-rank structure of tensors, but also takes into account the spatio-temporal characteristics of the data. Finally, we report numerical results on completing image, video and internet traffic data. The results demonstrate that our method outperforms some existing methods.

Keywords Tensor completion · Tensor factorization · Tensor fibered rank · Spatio-temporal characteristics

Mathematics Subject Classification 15A69 · 46B28

Communicated by Hedy Attouch.

✉ Xinzhen Zhang
xzzhang@tju.edu.cn

Quan Yu
quanyu@hnu.edu.cn

Zheng-Hai Huang
huangzhenghai@tju.edu.cn

[1] School of Mathematics, Hunan University, Changsha 410082, Hunan, China

[2] School of Mathematics, Tianjin University, Tianjin 300354, China

Published online: 05 September 2023

1 Introduction

A tensor is a multidimensional array, and an Nth-order tensor is an element of the tensor product space of N vector spaces, each with its own dimension [19]. Tensors, as higher-order generalizations of vectors and matrices, have wide applications in various fields [4, 8–10, 15, 21, 23, 27, 31, 36, 42]. Tensor decompositions, which are various generalizations of matrix singular value decomposition, have attracted more and more attention, including CANDECOMP/PARAFAC (CP) decomposition [7, 16], Tucker decomposition [35] and tensor singular value decomposition (SVD) [11, 13, 17, 18, 28]. Corresponding to such tensor decompositions, tensor ranks are called the CP rank, Tucker rank and tubal rank, respectively.

Third-order tensors are widely used in chemometrics [6, 30], psychometrics [20] and image inpainting [5, 24, 26, 48]. Unless otherwise specified, tensors in this paper are of third-order tensors. For a third-order (n_1, n_2, n_3)-dimensional tensor $\mathcal{C} \in \mathbb{R}^{n_1 \times n_2 \times n_3}$, the CP decomposition is to decompose $\mathcal{C}$ as a sum of some outer products of three vectors:

$$\mathcal{C} = \sum_{i=1}^{r} a_1^{(i)} \circ a_2^{(i)} \circ a_3^{(i)},$$

where the symbol "$\circ$" denotes the outer product and $a_j^{(i)} \in \mathbb{R}^{n_j}$ is a vector ($i \in \{1, 2, \ldots, r\}$ and $j \in \{1, 2, 3\}$). The smallest r in CP decomposition is called CP rank of $\mathcal{C}$. From [12], it is NP-hard to determine the CP rank. Compared with CP rank, Tucker rank is easy to compute, and hence most of low-rank tensor completion and recovery models are based on Tucker rank. Precisely, Tucker rank is a vector of the matrix ranks:

$$\text{rank}_{TC}(\mathcal{C}) = \left(\text{rank}(C_{(1)}), \text{rank}(C_{(2)}), \text{rank}(C_{(3)})\right),$$

where $C_{(1)} \in \mathbb{R}^{n_1 \times (n_2 n_3)}$ ($C_{(2)} \in \mathbb{R}^{n_2 \times (n_1 n_3)}$ and $C_{(3)} \in \mathbb{R}^{n_3 \times (n_1 n_2)}$) is mode-1 (mode-2 and mode-3, respectively) matricization of the tensor $\mathcal{C}$. More recently, Kilmer et al. [17] introduced tensor-tensor product (t-product) and tensor singular value decomposition (t-SVD). Based on these definitions, tubal rank was introduced and studied in [17, 18, 28]. More recently, tensor fibered rank was introduced by extending tubal rank and studied in [46].

The low-rank tensor completion problem is to find a low-rank tensor from observed incomplete data, which arises from various fields including internet traffic recovery [1, 2, 33, 47], image and video inpainting [14, 22, 23, 42, 48]. Low-rank tensor completion is modeled as

$$\min_{\mathcal{C}} \text{rank}(\mathcal{C}), \quad \text{s.t.} \quad P_{\Omega}(\mathcal{C}) = P_{\Omega}(\mathcal{M}), \tag{1}$$

where $\text{rank}(\cdot)$ is a tensor rank and Ω is an index set locating the observed data. P_{Ω} is a linear operator that extracts the entries in Ω and fills the entries not in Ω with zeros, and $\mathcal{M}$ is a given tensor.

Different tensor ranks lead to different low-rank tensor completion models of (1) with different methods. One of them is the well-known low-Tucker-rank tensor completion of the following form:

$$\min_{\mathcal{C}} \left(\operatorname{rank}(C_{(1)}),\ \operatorname{rank}(C_{(2)}),\ \operatorname{rank}(C_{(3)})\right), \quad \text{s.t.} \quad P_{\Omega}(\mathcal{C}) = P_{\Omega}(\mathcal{M}).$$

To keep things simple, the weighted Tucker rank minimization problems is formulated as

$$\min_{\mathcal{C}} \sum_{i=1}^{3} \alpha_i \operatorname{rank}(C_{(i)}), \quad \text{s.t.} \quad P_{\Omega}(\mathcal{C}) = P_{\Omega}(\mathcal{M}). \tag{2}$$

Note that problem (2) is nonconvex since the matrix rank function is nonconvex. To solve (2), the convex optimization problem is considered as

$$\min_{\mathcal{C}} \sum_{i=1}^{3} \alpha_i \left\| C_{(i)} \right\|_*, \quad \text{s.t.} \quad P_{\Omega}(\mathcal{C}) = P_{\Omega}(\mathcal{M}). \tag{3}$$

In general, SVD is needed in each iteration of numerical methods for (3), which leads to high computational cost. To lower the computational cost, a matrix factorization method was considered by Xu et al. [40], which preserves the low-rank structure of a matrix. Specifically, (2) is reformulated as

$$\min_{X^i, Y^i, \mathcal{C}} \sum_{i=1}^{3} \alpha_i \left\| X^i Y^i - C_{(i)} \right\|_F^2, \quad \text{s.t.} \quad P_{\Omega}(\mathcal{C}) = P_{\Omega}(\mathcal{M}). \tag{4}$$

This method has been widely used in various areas [25]. As pointed out in [17, 18, 28], unfolding a tensor directly will destroy the original multi-way structure of the data, which leads to vital information loss and degraded performance. Note that the sizes of $C_{(i)}$, $i = 1, 2, 3$ in (4) are the same as $\mathcal{C}$ in principle, which makes it difficult to lower the computational efforts.

Based on tubal rank, the following model was considered in [48] based on tensor factorization:

$$\min_{\mathcal{X}, \mathcal{Y}, \mathcal{C}} \frac{1}{2} \left\| \mathcal{X} * \mathcal{Y} - \mathcal{C} \right\|_F^2, \quad \text{s.t.} \quad P_{\Omega}(\mathcal{C} - \mathcal{M}) = 0, \tag{5}$$

where "$*$" denotes the tensor-tensor product (t-product). According to the analysis in [17, 18, 28, 48], the t-product can be computed by some block diagonal matrices of smaller sizes, which makes a significant reduction in computational cost. Later, a corrected tensor nuclear norm minimization method was developed in [44] for noisy observations. Furthermore, based on fibered rank, an efficient alternating direction method of multipliers (ADMMs)-based algorithm was proposed in hyperspectral image (HSI) denoising [46].

To make full use of the intrinsic spatio-temporal characteristics in image, video and internet traffic tensor completion, we introduce the low-fibered-rank tensor completion model that can better incorporate these characteristics than the tubal rank model. Then, we apply a tensor factorization-based method to solve this model. As far as we know, this paper is the first one to use priori information of spatio-temporal characteristics for image and video data recovery. Our numerical examples show that our results have higher peak signal-to-noise ratio (PSNR), structural similarity (SSIM) and feature similarity (FSIM) [43] than some existing methods, demonstrating the superiority of our model and method.

The paper is organized as follows. Section 2 presents preliminary knowledge on tensor fibered rank. In Sect. 3, we introduce a low tensor fibered rank tensor completion model for tensor data with some characteristics, and propose a tensor factorization-based method with its convergence analysis. Section 4 reports some numerical results on color image, gray video and internet traffic data recovery, demonstrating the efficiency of the proposed method. Section 5 briefly concludes our study.

2 Preliminary Knowledge

Before proceeding, we first present some notations here. For a positive integer n, $[\mathbf{n}] := \{1, 2, \ldots, n\}$. Scalars, vectors and matrices are denoted as lowercase letters $(a, b, c, \ldots)$, boldface lowercase letters $(\boldsymbol{a}, \boldsymbol{b}, \boldsymbol{c}, \ldots)$ and uppercase letters $(A, B, C, \ldots)$, respectively. Third-order tensors are denoted as calligraphic letters $(\mathcal{A}, \mathcal{B}, \mathcal{C}, \ldots)$, and the set of all the third-order real tensors is denoted as $\mathbb{R}^{n_1 \times n_2 \times n_3}$. For a third-order tensor $\mathcal{A} = (\mathcal{A}_{ijk}) \in \mathbb{R}^{n_1 \times n_2 \times n_3}$, $i \in [\mathbf{n_1}]$, $j \in [\mathbf{n_2}]$ and $k \in [\mathbf{n_3}]$, we use the Matlab notations $\mathcal{A}(i, :, :)$, $\mathcal{A}(:, j, :)$ and $\mathcal{A}(:, :, k)$ to denote its ith horizontal, jth lateral and kth frontal slice, respectively. Without confusion, we use $\mathcal{A}_{ijk}$ and $\mathcal{A}(i, j, k)$ to denote the (i, j, k)th entries of $\mathcal{A}$. Then, we denote

$$A_1^{(i)} := \mathcal{A}(i, :, :),\ A_2^{(j)} := \mathcal{A}(:, j, :),\ A_3^{(k)} := \mathcal{A}(:, :, k).$$

The inner product of two tensors $\mathcal{A}, \mathcal{B} \in \mathbb{R}^{n_1 \times n_2 \times n_3}$ is the sum of products of their entries, i.e.,

$$\langle \mathcal{A}, \mathcal{B} \rangle = \sum_{i=1}^{n_1} \sum_{j=1}^{n_2} \sum_{k=1}^{n_3} \mathcal{A}_{ijk} \mathcal{B}_{ijk}.$$

The Frobenius norm is defined as $\|\mathcal{A}\|_F = \sqrt{\langle \mathcal{A}, \mathcal{A} \rangle}$. For a matrix A, A^H and A^{-1} represent the conjugate transpose and the inverse of A, respectively. I represents the identity matrix. For any $u \in [\mathbf{3}]$, the u-mode matrix product of a tensor $\mathcal{A} = (\mathcal{A}_{ijk}) \in \mathbb{R}^{n_1 \times n_2 \times n_3}$ with a matrix $M_u \in \mathbb{R}^{J \times n_u}$ is denoted by $\mathcal{A} \times_u M_u$ with its entries

$$\begin{aligned}
(\mathcal{A} \times_1 M_1)_{i_1 jk} &= \textstyle\sum_{i=1}^{n_1} \mathcal{A}_{ijk} (M_1)_{i_1 i}, \\
(\mathcal{A} \times_2 M_2)_{i j_1 k} &= \textstyle\sum_{j=1}^{n_2} \mathcal{A}_{ijk} (M_2)_{j_1 j}, \\
(\mathcal{A} \times_3 M_3)_{ijk_1} &= \textstyle\sum_{k=1}^{n_3} \mathcal{A}_{ijk} (M_3)_{k_1 k}.
\end{aligned}$$

Now we are ready to recall tensor fibered rank, which is a generalization of tubal rank in [17]. Before proceeding, we review the Discrete Fourier Transformation (DFT), which plays a key role in t-product. For $\mathcal{A} \in \mathbb{R}^{n_1\times n_2\times n_3}$ and $u \in [\mathbf{3}]$, let $\bar{\mathcal{A}}_u \in \mathbb{C}^{n_1\times n_2\times n_3}$ be the result of DFT of $\mathcal{A} \in \mathbb{R}^{n_1\times n_2\times n_3}$ along the uth mode. Specifically, let $F_{n_u} = [\boldsymbol{f_1}, \ldots, \boldsymbol{f_{n_u}}] \in \mathbb{C}^{n_u\times n_u}$, where $\boldsymbol{f_i} = \left[1; \omega^{(i-1)}; \ldots; \omega^{k(i-1)}; \ldots; \omega^{(n_u-1)(i-1)}\right] \in \mathbb{C}^{n_u}$ with $\omega = e^{-\frac{2\pi \mathfrak{b}}{n_u}}$ and $\mathfrak{b} = \sqrt{-1}$. Then

$$\bar{\mathcal{A}}_1(:, j, k) = F_{n_1}\mathcal{A}(:, j, k), \quad \bar{\mathcal{A}}_2(i, :, k) = F_{n_2}\mathcal{A}(i, :, k), \quad \bar{\mathcal{A}}_3(i, j, :) = F_{n_3}\mathcal{A}(i, j, :),$$

which can be computed by Matlab command "$\bar{\mathcal{A}}_u = fft(\mathcal{A}, [\,], u)$". Furthermore, $\mathcal{A}$ can be computed by $\bar{\mathcal{A}}_u$ with the inverse DFT $\mathcal{A} = ifft(\bar{\mathcal{A}}_u, [\,], u)$.

For $\mathcal{A} \in \mathbb{R}^{n_1\times n_2\times n_3}$, we define matrices $\bar{A}_1 \in \mathbb{C}^{n_1n_2\times n_1n_3}$, $\bar{A}_2 \in \mathbb{C}^{n_1n_2\times n_2n_3}$ and $\bar{A}_3 \in \mathbb{C}^{n_1n_3\times n_2n_3}$ as

$$\begin{aligned}\bar{A}_u &= bdiag_u\left(\bar{\mathcal{A}}_u\right)\\ &= \begin{bmatrix} \bar{A}_u^{(1)} & & & \\ & \bar{A}_u^{(2)} & & \\ & & \ddots & \\ & & & \bar{A}_u^{(n_u)} \end{bmatrix}, \quad \forall\, u \in [\mathbf{3}]. \end{aligned} \tag{6}$$

Here, $bdiag_u(\cdot)$ is an operator which maps the tensor $\bar{\mathcal{A}}_u$ to the block diagonal matrix $\bar{A}_u$. The block circulant matrices $bcirc_1(\mathcal{A}) \in \mathbb{R}^{n_1n_2\times n_1n_3}$, $bcirc_2(\mathcal{A}) \in \mathbb{R}^{n_1n_2\times n_2n_3}$ and $bcirc_3(\mathcal{A}) \in \mathbb{R}^{n_1n_3\times n_2n_3}$ of $\mathcal{A}$ are defined as

$$bcirc_u(\mathcal{A}) = \begin{bmatrix} A_u^{(1)} & A_u^{(n_u)} & \cdots & A_u^{(2)} \\ A_u^{(2)} & A_u^{(1)} & \cdots & A_u^{(3)} \\ \vdots & \vdots & \ddots & \vdots \\ A_u^{(n_u)} & A_u^{(n_u-1)} & \cdots & A_u^{(1)} \end{bmatrix}, \quad \forall\, u \in [\mathbf{3}].$$

Based on these notations, mode-k t-product, mode-k fibered rank and tensor fibered rank were introduced in [46].

Definition 1 (*Mode-k t-product*) For $\mathcal{A}_1 \in \mathbb{R}^{n_1\times n_2\times r_1}$ and $\mathcal{B}_1 \in \mathbb{R}^{n_1\times r_1\times n_3}$, define

$$\mathcal{A}_1 *_1 \mathcal{B}_1 := fold_1(bcirc_1(\mathcal{A}_1) \cdot unfold_1(\mathcal{B}_1)) \in \mathbb{R}^{n_1\times n_2\times n_3}.$$

For $\mathcal{A}_2 \in \mathbb{R}^{n_1\times n_2\times r_2}$ and $\mathcal{B}_2 \in \mathbb{R}^{r_2\times n_2\times n_3}$, define

$$\mathcal{A}_2 *_2 \mathcal{B}_2 := fold_2(bcirc_2(\mathcal{A}_2) \cdot unfold_2(\mathcal{B}_2)) \in \mathbb{R}^{n_1\times n_2\times n_3}.$$

For $\mathcal{A}_3 \in \mathbb{R}^{n_1\times r_3\times n_3}$ and $\mathcal{B}_3 \in \mathbb{R}^{r_3\times n_2\times n_3}$, define

$$\mathcal{A}_3 *_3 \mathcal{B}_3 := fold_3(bcirc_3(\mathcal{A}_3) \cdot unfold_3(\mathcal{B}_3)) \in \mathbb{R}^{n_1\times n_2\times n_3}.$$

Here

$$unfold_u(\mathcal{B}_u) = [B_u^{(1)}; B_u^{(2)}; \ldots; B_u^{(n_u)}],$$

and its inverse operator "$fold_u$" is defined by $fold_u(unfold_u(\mathcal{B}_u)) = \mathcal{B}_u$.

Definition 2 (*Tensor fibered rank and mode-k fibered rank*) For any tensor $\mathcal{A} \in \mathbb{R}^{n_1 \times n_2 \times n_3}$ and $u \in [\mathbf{3}]$, let $r_u^l = \text{rank}(\bar{A}_u^{(l)})$ and $l \in [\mathbf{n_u}]$. Then tensor fibered rank of $\mathcal{A}$ is defined as a vector

$$rank_f(\mathcal{A}) = (r_1(\mathcal{A}), r_2(\mathcal{A}), r_3(\mathcal{A})),$$

where $r_u(\mathcal{A}) = \max\{r_u^1, r_u^2, \ldots, r_u^{n_u}\}$ for $u \in [\mathbf{3}]$ is called the mode-k fibered rank.

For mode-k t-product, we have the following result, which is due to [18, 48].

Lemma 1 *Suppose that $\mathcal{A}$, $\mathcal{B}$ are tensors such that $\mathcal{F} := \mathcal{A} *_u \mathcal{B}$ ($u \in [\mathbf{3}]$) is well defined as in Definition 1. Let $\bar{A}_u$, $\bar{B}_u$, $\bar{F}_u$ be defined as in (6) and $r_u(\cdot)$ be defined as in Definition 2. Then*

(1) $\|\mathcal{A}\|_F^2 = \frac{1}{n_u} \|\bar{A}_u\|_F^2$;
(2) $\mathcal{F} = \mathcal{A} *_u \mathcal{B}$ *and* $\bar{F}_u = \bar{A}_u \bar{B}_u$ *are equivalent;*
(3) $r_u(\mathcal{F}) \leq \min\{r_u(\mathcal{A}), r_u(\mathcal{B})\}$.

From Lemma 1, we can assert that the generalized tensor factorization can be computed by matrix factorization, which is computable.

3 Low-Rank Tensor Completion of Third-Order Tensors with Spatio-temporal Characteristics

In practical applications, some characteristics of the data are included in the tensor completion problem. For example, both the video data between the two adjacent frames and the internet traffic data between two adjacent days have temporal stability features. To characterize such properties, some constraint matrices are considered.

As in [32, 47], the temporal constraint matrix H captures the temporal stability feature, i.e., the data is similar at two adjacent time slots in the tensor. Specifically, let n_3 be the time dimension and $H = Toeplitz(0, 1, -1)$ be a Toeplitz matrix of size $(n_3 - 1) \times n_3$ with

$$H = \begin{bmatrix} 1 & -1 & 0 & \cdots & 0 \\ 0 & 1 & -1 & \cdots & 0 \\ \vdots & \vdots & \vdots & \ddots & \vdots \\ 0 & 0 & 0 & \cdots & -1 \end{bmatrix}_{(n_3-1)\times n_3}.$$

Then the time stability is expressed by minimizing $\|\mathcal{C} \times_3 H\|_F^2 = \sum_{k=1}^{n_3-1} \left\| \mathcal{C}_3^{(k)} - \mathcal{C}_3^{(k+1)} \right\|_F^2$. That is, we get an approximation that has the similar temporally

adjacent values. Similarly, let the spatial constraint matrices F and G capture spatial correlation feature [47]. We choose F and G according to the similarity between $\mathcal{C}_1^{(i)}$ and $\mathcal{C}_1^{(j)}$ $(j \neq i)$, $\mathcal{C}_2^{(i)}$ and $\mathcal{C}_2^{(j)}$ $(j \neq i)$, respectively. For each $\mathcal{C}_1^{(i)}$, we perform linear regression to find a set of weights $w_i(j)$ such that the linear combination of $\mathcal{C}_1^{(j)}$ is a best approximation of $\mathcal{C}_1^{(i)}$, i.e., $\mathcal{C}_1^{(i)} = \sum_{j \neq i} w_i(j)\mathcal{C}_1^{(j)}$. Then we set $F(i,i) = 1$ and $F(i,j) = -w_i(j)$. Matrix G can be obtained similarly. Let n_1 and n_2 be the spatial dimensions. Then the spatial correlation features can be expressed by minimizing

$$\|\mathcal{C} \times_1 F\|_F^2 = \sum_{i=1}^{n_1} \left\| C_1^{(i)} - \sum_{j \neq i} w_i(j) C_1^{(j)} \right\|_F^2,$$

$$\|\mathcal{C} \times_2 G\|_F^2 = \sum_{i=1}^{n_2} \left\| C_2^{(i)} - \sum_{j \neq i} w_i(j) C_2^{(j)} \right\|_F^2.$$

Before we get such matrices F and G, it is necessary to estimate an initial tensor $\mathcal{C}$ without missing data and outliers because these factors may destroy spatial features. To this end, we first recover the missing entries and remove outliers by using the temporal constraint (i.e., H). For the estimated tensor $\mathcal{C}$, we analyze the similarities and linear regression to find spatial constraints (i.e., F, G). Then the obtained F, G are used together with matrix H in algorithm to recovery the data.

3.1 Tensor Factorization-Based Method

Consider the following low-rank tensor completion model based on tensor fibered rank

$$\min_{\mathcal{C}} \operatorname{rank}_f(\mathcal{C}), \quad \text{s.t.} \quad P_\Omega(\mathcal{C} - \mathcal{M}) = 0.$$

Based on mode-k t-product, the low tensor fibered rank completion model can be approximated by

$$\min_{\mathcal{X}_u, \mathcal{Y}_u, \mathcal{C}} \sum_{u=1}^{3} \frac{\alpha_u}{2} \|\mathcal{X}_u *_u \mathcal{Y}_u - \mathcal{C}\|_F^2, \quad \text{s.t.} \quad P_\Omega(\mathcal{C} - \mathcal{M}) = 0.$$

For the three suitable matrices F, G and H, we propose a low-rank tensor completion model for tensor data with spatio-temporal characteristics using tensor factorization:

$$\begin{aligned}\min_{\mathcal{X}_u,\mathcal{Y}_u,\mathcal{C}} &\sum_{u=1}^{3}\frac{\alpha_u}{2}\|\mathcal{X}_u *_u \mathcal{Y}_u - \mathcal{C}\|_F^2 + \frac{\beta_1}{2}\|(\mathcal{X}_2 *_2 \mathcal{Y}_2)\times_1 F\|_F^2 + \frac{\beta_2}{2}\|(\mathcal{X}_3 *_3 \mathcal{Y}_3)\times_2 G\|_F^2 \\ &+\frac{\beta_3}{2}\|(\mathcal{X}_1 *_1 \mathcal{Y}_1)\times_3 H\|_F^2 \\ \text{s.t.}\quad & P_\Omega(\mathcal{C}-\mathcal{M}) = 0. \end{aligned} \tag{7}$$

Let $\beta_u = 0$ if there are no additional characteristics on the uth dimension of data.

Now we present the following lemma, which is helpful to solve problem (7).

Lemma 2 *Suppose that* $\mathcal{C}\in\mathbb{R}^{n_1\times n_2\times n_3}$, $F\in\mathbb{R}^{n_1\times n_1}$, $G\in\mathbb{R}^{n_2\times n_2}$ *and* $H\in\mathbb{R}^{n_3\times n_3}$. *Let* $\mathcal{F}\in\mathbb{R}^{n_1\times n_2\times n_1}$, $\tilde{\mathcal{F}}\in\mathbb{R}^{n_1\times n_1\times n_3}$, $\mathcal{G}\in\mathbb{R}^{n_2\times n_2\times n_3}$, $\tilde{\mathcal{G}}\in\mathbb{R}^{n_1\times n_2\times n_2}$, $\mathcal{H}\in\mathbb{R}^{n_1\times n_3\times n_3}$, $\tilde{\mathcal{H}}\in\mathbb{R}^{n_3\times n_2\times n_3}$ *be the tensors with their slices*

$$\begin{aligned} &F_2^{(1)} = F,\ F_2^{(2)} = \cdots = F_2^{(n_2)} = 0, \quad \tilde{F}_3^{(1)} = F,\ \tilde{F}_3^{(2)} = \cdots = \tilde{F}_3^{(n_3)} = 0,\\ &G_3^{(1)} = G^H,\ G_3^{(2)} = \cdots = G_3^{(n_3)} = 0, \quad \tilde{G}_1^{(1)} = G,\ \tilde{G}_1^{(2)} = \cdots = \tilde{G}_1^{(n_1)} = 0,\\ &H_1^{(1)} = H^H,\ H_1^{(2)} = \cdots = H_1^{(n_1)} = 0, \quad \tilde{H}_2^{(1)} = H^H,\ \tilde{H}_2^{(2)} = \cdots = \tilde{H}_2^{(n_2)} = 0. \end{aligned}$$

Then

$$\begin{cases}\mathcal{F}*_2\mathcal{C} = \mathcal{C}\times_1 F,\\ \tilde{\mathcal{F}}*_3\mathcal{C} = \mathcal{C}\times_1 F,\end{cases} \quad \begin{cases}\mathcal{C}*_3\mathcal{G} = \mathcal{C}\times_2 G,\\ \tilde{\mathcal{G}}*_1\mathcal{C} = \mathcal{C}\times_2 G,\end{cases} \quad \begin{cases}\mathcal{C}*_1\mathcal{H} = \mathcal{C}\times_3 H,\\ \mathcal{C}*_2\tilde{\mathcal{H}} = \mathcal{C}\times_3 H.\end{cases}$$

Proof It is clear to see that

$$\begin{aligned} &unfold_2(\mathcal{F}*_2\mathcal{C}) = bcirc_2(\mathcal{F})\cdot unfold_2(\mathcal{C})\\ &= \begin{bmatrix} F_2^{(1)} & F_2^{(n_2)} & \cdots & F_2^{(2)}\\ F_2^{(2)} & F_2^{(1)} & \cdots & F_2^{(3)}\\ \vdots & \vdots & \ddots & \vdots\\ F_2^{(n_2)} & F_2^{(n_2-1)} & \cdots & F_2^{(1)}\end{bmatrix}\begin{bmatrix} C_2^{(1)}\\ C_2^{(2)}\\ \vdots\\ C_2^{(n_2)}\end{bmatrix} = \begin{bmatrix} F & 0 & \cdots & 0\\ 0 & F & \cdots & 0\\ \vdots & \vdots & \ddots & \vdots\\ 0 & 0 & \cdots & F\end{bmatrix}\begin{bmatrix} C_2^{(1)}\\ C_2^{(2)}\\ \vdots\\ C_2^{(n_2)}\end{bmatrix} = \begin{bmatrix} FC_2^{(1)}\\ FC_2^{(2)}\\ \vdots\\ FC_2^{(n_2)}\end{bmatrix}. \end{aligned}$$

Then

$$(\mathcal{F}*_2\mathcal{C})_{ijk} = \left(FC_2^{(j)}\right)_{ik} = \sum_{p=1}^{n_1} F_{ip}\left(C_2^{(j)}\right)_{pk} = \sum_{p=1}^{n_1}\mathcal{C}_{pjk}F_{ip} = (\mathcal{C}\times_1 F)_{ijk}.$$

Similarly,

$$\left(\tilde{\mathcal{F}}*_3\mathcal{C}\right)_{ijk} = \left(FC_3^{(k)}\right)_{ij} = \sum_{p=1}^{n_1} F_{ip}\left(C_3^{(k)}\right)_{pj} = \sum_{p=1}^{n_1}\mathcal{C}_{pjk}F_{ip} = (\mathcal{C}\times_1 F)_{ijk}.$$

Now we can assert that $\mathcal{F}*_2\mathcal{C} = \mathcal{C}\times_1 F$ and $\tilde{\mathcal{F}}*_3\mathcal{C} = \mathcal{C}\times_1 F$.

Furthermore,

$$\begin{aligned} unfold_3\left(\mathcal{C}*_3\mathcal{G}\right) &= bcirc_3\left(\mathcal{C}\right)\cdot unfold_3\left(\mathcal{G}\right) \\ &= \begin{bmatrix} C_3^{(1)} & C_3^{(n_3)} & \cdots & C_3^{(2)} \\ C_3^{(2)} & C_3^{(1)} & \cdots & C_3^{(3)} \\ \vdots & \vdots & \ddots & \vdots \\ C_3^{(n_3)} & C_3^{(n_3-1)} & \cdots & C_3^{(1)} \end{bmatrix} \begin{bmatrix} G_3^{(1)} \\ G_3^{(2)} \\ \vdots \\ G_3^{(n_3)} \end{bmatrix} \\ &= \begin{bmatrix} C_3^{(1)} & C_3^{(n_3)} & \cdots & C_3^{(2)} \\ C_3^{(2)} & C_3^{(1)} & \cdots & C_3^{(3)} \\ \vdots & \vdots & \ddots & \vdots \\ C_3^{(n_3)} & C_3^{(n_3-1)} & \cdots & C_3^{(1)} \end{bmatrix} \begin{bmatrix} G^H \\ 0 \\ \vdots \\ 0 \end{bmatrix} = \begin{bmatrix} C_3^{(1)}G^H \\ C_3^{(2)}G^H \\ \vdots \\ C_3^{(n_3)}G^H \end{bmatrix}. \end{aligned}$$

Then

$$\left(\mathcal{C}*_3\mathcal{G}\right)_{ijk} = \left(C_3^{(k)}G^H\right)_{ij} = \sum_{p=1}^{n_2}\left(C_3^{(k)}\right)_{ip}\left(G^H\right)_{pj} = \sum_{p=1}^{n_2}\mathcal{C}_{ipk}G_{jp} = \left(\mathcal{C}\times_2 G\right)_{ijk}.$$

Similarly,

$$\left(\tilde{\mathcal{G}}*_1\mathcal{C}\right)_{ijk} = \left(GC_1^{(i)}\right)_{jk} = \sum_{p=1}^{n_2}\left(G\right)_{jp}\left(C_1^{(i)}\right)_{pk} = \sum_{p=1}^{n_2}\mathcal{C}_{ipk}G_{jp} = \left(\mathcal{C}\times_2 G\right)_{ijk}.$$

Then $\mathcal{C}*_3\mathcal{G} = \mathcal{C}\times_2 G$ and $\tilde{\mathcal{G}}*_1\mathcal{C} = \mathcal{C}\times_2 G$. Similarly, $\mathcal{C}*_1\mathcal{H} = \mathcal{C}\times_3 H$ and $\mathcal{C}*_2\tilde{\mathcal{H}} = \mathcal{C}\times_3 H$. Hence the desired results are arrived. □

With Lemma 2, (7) can be rewritten as

$$\begin{aligned} \min_{\mathcal{X}_u,\mathcal{Y}_u,\mathcal{C}} \ & \sum_{u=1}^{3}\tfrac{\alpha_u}{2}\left\|\mathcal{X}_u*_u\mathcal{Y}_u-\mathcal{C}\right\|_F^2+\tfrac{\beta_1}{2}\left\|\mathcal{F}*_2\left(\mathcal{X}_2*_2\mathcal{Y}_2\right)\right\|_F^2+\tfrac{\beta_2}{2}\left\|\left(\mathcal{X}_3*_3\mathcal{Y}_3\right)*_3\mathcal{G}\right\|_F^2 \\ & +\tfrac{\beta_3}{2}\left\|\left(\mathcal{X}_1*_1\mathcal{Y}_1\right)*_1\mathcal{H}\right\|_F^2 \\ \text{s.t.} \ & P_{\Omega}(\mathcal{C}-\mathcal{M})=0. \end{aligned} \tag{8}$$

To ascertain the factors without scaling, additional regularized terms are added in the objective function, denoted by $f(\mathcal{C},\mathcal{X}_1,\mathcal{X}_2,\mathcal{X}_3,\mathcal{Y}_1,\mathcal{Y}_2,\mathcal{Y}_3)$. Consider the following regularized version of problem (8)

$$\min_{\mathcal{C},\mathcal{X}_u,\mathcal{Y}_u} f(\mathcal{C},\mathcal{X}_1,\mathcal{X}_2,\mathcal{X}_3,\mathcal{Y}_1,\mathcal{Y}_2,\mathcal{Y}_3), \quad \text{s.t.} \quad P_{\Omega}(\mathcal{C}-\mathcal{M})=0, \tag{9}$$

where

$$
\begin{aligned}
&f(\mathcal{C}, \mathcal{X}_1, \mathcal{X}_2, \mathcal{X}_3, \mathcal{Y}_1, \mathcal{Y}_2, \mathcal{Y}_3) \\
&= \sum_{u=1}^{3} \frac{\alpha_u}{2} \|\mathcal{X}_u *_u \mathcal{Y}_u - \mathcal{C}\|_F^2 + \frac{\beta_1}{2} \|\mathcal{F} *_2 (\mathcal{X}_2 *_2 \mathcal{Y}_2)\|_F^2 + \frac{\beta_2}{2} \|(\mathcal{X}_3 *_3 \mathcal{Y}_3) *_3 \mathcal{G}\|_F^2 \\
&\quad + \frac{\beta_3}{2} \|(\mathcal{X}_1 *_1 \mathcal{Y}_1) *_1 \mathcal{H}\|_F^2 \\
&\quad + \frac{\lambda}{2} \left(\beta_1 \|\mathcal{F} *_2 \mathcal{X}_2\|_F^2 + \alpha_2 \|\mathcal{X}_2\|_F^2 + \|\mathcal{Y}_2\|_F^2 \right) \\
&\quad + \frac{\lambda}{2} \left(\|\mathcal{X}_3\|_F^2 + \beta_2 \|\mathcal{Y}_3 *_3 \mathcal{G}\|_F^2 + \alpha_3 \|\mathcal{Y}_3\|_F^2 \right) \\
&\quad + \frac{\lambda}{2} \left(\|\mathcal{X}_1\|_F^2 + \beta_3 \|\mathcal{Y}_1 *_1 \mathcal{H}\|_F^2 + \alpha_1 \|\mathcal{Y}_1\|_F^2 \right).
\end{aligned}
$$

Now we update $\mathcal{C}$, $\mathcal{X}_u$, $\mathcal{Y}_u$ alternatively. Note that

$$
\begin{aligned}
&\sum_{u=1}^{3} \alpha_u \|\mathcal{X}_u *_u \mathcal{Y}_u - \mathcal{C}\|_F^2 = \sum_{u=1}^{3} \alpha_u \langle \mathcal{X}_u *_u \mathcal{Y}_u - \mathcal{C}, \mathcal{X}_u *_u \mathcal{Y}_u - \mathcal{C} \rangle \\
&= \sum_{u=1}^{3} \alpha_u \langle \mathcal{C}, \mathcal{C} \rangle - 2 \sum_{u=1}^{3} \alpha_u \langle \mathcal{X}_u *_u \mathcal{Y}_u, \mathcal{C} \rangle + \sum_{u=1}^{3} \alpha_u \langle \mathcal{X}_u *_u \mathcal{Y}_u, \mathcal{X}_u *_u \mathcal{Y}_u \rangle \\
&= \langle \mathcal{C}, \mathcal{C} \rangle - 2 \left\langle \sum_{u=1}^{3} \alpha_u \mathcal{X}_u *_u \mathcal{Y}_u, \mathcal{C} \right\rangle + \sum_{u=1}^{3} \alpha_u \|\mathcal{X}_u *_u \mathcal{Y}_u\|_F^2 \\
&= \left\langle \sum_{u=1}^{3} \alpha_u \mathcal{X}_u *_u \mathcal{Y}_u - \mathcal{C}, \sum_{u=1}^{3} \alpha_u \mathcal{X}_u *_u \mathcal{Y}_u - \mathcal{C} \right\rangle + \sum_{u=1}^{3} \alpha_u \|\mathcal{X}_u *_u \mathcal{Y}_u\|_F^2 - \left\| \sum_{u=1}^{3} \alpha_u \mathcal{X}_u *_u \mathcal{Y}_u \right\|_F^2 \\
&= \left\| \sum_{u=1}^{3} \alpha_u \mathcal{X}_u *_u \mathcal{Y}_u - \mathcal{C} \right\|_F^2 + \sum_{u=1}^{3} \alpha_u \|\mathcal{X}_u *_u \mathcal{Y}_u\|_F^2 - \left\| \sum_{u=1}^{3} \alpha_u \mathcal{X}_u *_u \mathcal{Y}_u \right\|_F^2. \qquad (10)
\end{aligned}
$$

Then $\mathcal{C}^{t+1}$ can be updated by

$$
\begin{aligned}
\mathcal{C}^{t+1} &= \underset{P_\Omega(\mathcal{C}-\mathcal{M})=0}{\operatorname{argmin}} \frac{1}{2} \left\| \sum_{u=1}^{3} \alpha_u \mathcal{X}_u^t *_u \mathcal{Y}_u^t - \mathcal{C} \right\|_F^2 \\
&= \sum_{u=1}^{3} \alpha_u \mathcal{X}_u^t *_u \mathcal{Y}_u^t + P_\Omega \left(\mathcal{M} - \sum_{u=1}^{3} \alpha_u \mathcal{X}_u^t *_u \mathcal{Y}_u^t \right). \qquad (11)
\end{aligned}
$$

Before we present how to update $\mathcal{X}_u^{t+1}$ and $\mathcal{Y}_u^{t+1}$, we rewrite (9) as a corresponding matrix version. Denote $r_u := r_u(\mathcal{C})$, $r_u^l := \operatorname{rank}(\bar{C}_u^{(l)})$ with $\bar{C}_u^{(l)} \in \mathbb{C}^{n_{u_1} \times n_{u_2}}$, $u_1 < u_2$ and $u_1, u_2 \neq u$. Clearly, $r_u^l \leq r_u$ for all $l \in [\mathbf{n_u}]$. For each u and l, $\bar{C}_u^{(l)}$ can be factorized as a product of two matrices $\hat{X}_u^{(l)}$ and $\hat{Y}_u^{(l)}$ of smaller sizes, where $\hat{X}_u^{(l)} \in \mathbb{C}^{n_{u_1} \times r_u^l}$ and $\hat{Y}_u^{(l)} \in \mathbb{C}^{r_u^l \times n_{u_2}}$ are the lth block diagonal matrices of $\hat{X}_u \in \mathbb{C}^{n_{u_1} n_u \times (\sum_{l=1}^{n_u} r_u^l)}$ and

$\hat{Y}_u \in \mathbb{C}^{(\sum_{l=1}^{n_u} r_u^l)\times n_u n_{u_2}}$. Let $\bar{X}_u^{(l)} = [\hat{X}_u^{(l)}, 0] \in \mathbb{C}^{n_{u_1}\times r_u}$, $\bar{Y}_u^{(l)} = [\hat{Y}_u^{(l)}; 0] \in \mathbb{C}^{r_u \times n_{u_2}}$ and $\bar{X}_u, \bar{Y}_u$ be the block diagonal matrices with the lth block diagonal matrices $\bar{X}_u^{(l)}, \bar{Y}_u^{(l)}$, respectively. Then $\hat{X}_u\hat{Y}_u = \bar{X}_u\bar{Y}_u$. Together with Lemma 1, we have

$$\begin{aligned}\|\mathcal{F} *_2 (\mathcal{X}_2 *_2 \mathcal{Y}_2)\|_F^2 &= \frac{1}{n_2}\|\bar{F}_2\overline{(\mathcal{X}_2 *_2 \mathcal{Y}_2)}\|_F^2 = \frac{1}{n_2}\|\bar{F}_2\left(\bar{X}_2\bar{Y}_2\right)\|_F^2 \\ &= \frac{1}{n_2}\|\bar{F}_2\left(\hat{X}_2\hat{Y}_2\right)\|_F^2 = \frac{1}{n_2}\|\bar{F}_2\hat{X}_2\hat{Y}_2\|_F^2 = \frac{1}{n_2}\sum_{j=1}^{n_2}\left\|\bar{F}_2^{(j)}\hat{X}_2^{(j)}\hat{Y}_2^{(j)}\right\|_F^2.\end{aligned}$$

Similarly, we have

$$\begin{aligned}\|(\mathcal{X}_3 *_3 \mathcal{Y}_3) *_3 \mathcal{G}\|_F^2 &= \frac{1}{n_3}\sum_{k=1}^{n_3}\left\|\hat{X}_3^{(k)}\hat{Y}_3^{(k)}\bar{G}_3^{(k)}\right\|_F^2, \\ \|(\mathcal{X}_1 *_1 \mathcal{Y}_1) *_1 \mathcal{H}\|_F^2 &= \frac{1}{n_1}\sum_{i=1}^{n_1}\left\|\hat{X}_1^{(i)}\hat{Y}_1^{(i)}\bar{H}_1^{(i)}\right\|_F^2.\end{aligned}$$

Based on these results, we can rewrite (9) as the following matrix version:

$$\begin{aligned}\min_{\mathcal{C},\hat{X}_u,\hat{Y}_u} &\sum_{l=1}^{n_u}\frac{\alpha_u}{2n_u}\left\|\hat{X}_u^{(l)}\hat{Y}_u^{(l)} - \bar{C}_u^{(l)}\right\|_F^2 + \frac{\beta_1}{2n_2}\sum_{j=1}^{n_2}\left\|\bar{F}_2^{(j)}\hat{X}_2^{(j)}\hat{Y}_2^{(j)}\right\|_F^2 \\ &+ \frac{\beta_2}{2n_3}\sum_{k=1}^{n_3}\left\|\hat{X}_3^{(k)}\hat{Y}_3^{(k)}\bar{G}_3^{(k)}\right\|_F^2 + \frac{\beta_3}{2n_1}\sum_{i=1}^{n_1}\left\|\hat{X}_1^{(i)}\hat{Y}_1^{(i)}\bar{H}_1^{(i)}\right\|_F^2 \\ &+ \lambda\left(\frac{\beta_1}{2n_2}\sum_{j=1}^{n_2}\left\|\bar{F}_2^{(j)}\hat{X}_2^{(j)}\right\|_F^2 + \frac{\alpha_2}{2n_2}\sum_{j=1}^{n_2}\left\|\hat{X}_2^{(j)}\right\|_F^2 + \frac{1}{2n_2}\sum_{j=1}^{n_2}\left\|\hat{Y}_2^{(j)}\right\|_F^2\right) \\ &+ \lambda\left(\frac{1}{2n_3}\sum_{k=1}^{n_3}\left\|\hat{X}_3^{(k)}\right\|_F^2 + \frac{\beta_2}{2n_3}\sum_{k=1}^{n_3}\left\|\hat{Y}_3^{(k)}\hat{G}_3^{(k)}\right\|_F^2 + \frac{\alpha_3}{2n_3}\sum_{k=1}^{n_3}\left\|\hat{Y}_3^{(k)}\right\|_F^2\right) \\ &+ \lambda\left(\frac{1}{2n_1}\sum_{i=1}^{n_1}\left\|\hat{X}_1^{(i)}\right\|_F^2 + \frac{\beta_3}{2n_1}\sum_{i=1}^{n_1}\left\|\hat{Y}_1^{(i)}\bar{H}_1^{(i)}\right\|_F^2 + \frac{\alpha_1}{2n_1}\sum_{i=1}^{n_1}\left\|\hat{Y}_1^{(i)}\right\|_F^2\right).\end{aligned}$$

To update $\hat{X}_1^{(i,t+1)}$, we consider its regularized version and have $\hat{X}_1^{(i,t+1)}$ as follows:

$$\begin{aligned}\hat{X}_1^{(i,t+1)} &= \underset{\hat{X}_1^{(i)}}{argmin}\ \frac{\alpha_1}{2n_1}\left\|\hat{X}_1^{(i)}\hat{Y}_1^{(i,t)} - \bar{C}_1^{(i,t+1)}\right\|_F^2 + \frac{\beta_3}{2n_1}\left\|\hat{X}_1^{(i)}\hat{Y}_1^{(i,t)}\bar{H}_1^{(i)}\right\|_F^2 + \frac{\lambda}{2n_1}\left\|\hat{X}_1^{(i)}\right\|_F^2 \\ &= \alpha_1\bar{C}_1^{(i,t+1)}\left(\hat{Y}_1^{(i,t)}\right)^H\left[\alpha_1\hat{Y}_1^{(i,t)}\left(\hat{Y}_1^{(i,t)}\right)^H + \beta_3\left(\hat{Y}_1^{(i,t)}\bar{H}_1^{(i)}\right)\left(\hat{Y}_1^{(i,t)}\bar{H}_1^{(i)}\right)^H + \lambda I\right]^{-1}.\end{aligned} \tag{12}$$

Similarly, $\hat{Y}_1^{(i,t+1)}$ can be updated by

$$\begin{aligned}\hat{Y}_1^{(i,t+1)} &= \underset{\hat{Y}_1^{(i)}}{argmin}\ \frac{\alpha_1}{2n_1}\left\|\hat{X}_1^{(i,t+1)}\hat{Y}_1^{(i)} - \bar{C}_1^{(i,t+1)}\right\|_F^2 + \frac{\beta_3}{2n_1}\left\|\hat{X}_1^{(i,t+1)}\hat{Y}_1^{(i,t)}\bar{H}_1^{(i)}\right\|_F^2 \\ &\quad + \frac{\lambda\beta_3}{2n_1}\left\|\hat{Y}_1^{(i)}\bar{H}_1^{(i)}\right\|_F^2 + \frac{\lambda\alpha_1}{2n_1}\left\|\hat{Y}_1^{(i)}\right\|_F^2 \\ &= \alpha_1\left[\left(\hat{X}_1^{(i,t+1)}\right)^H\hat{X}_1^{(i,t+1)} + \lambda I\right]^{-1}\left(\hat{X}_1^{(i,t+1)}\right)^H\bar{C}_1^{(i,t+1)} \\ &\quad \left[\alpha_1 I + \beta_3\bar{H}_1^{(i)}\left(\bar{H}_1^{(i)}\right)^H\right]^{-1}.\end{aligned} \tag{13}$$

Similarly, $\hat{X}_2^{(j,t+1)}$, $\hat{Y}_2^{(j,t+1)}$, $\hat{X}_3^{(k,t+1)}$, $\hat{Y}_3^{(k,t+1)}$ can be updated by

$$\hat{X}_2^{(j,t+1)} = \alpha_2\left[\alpha_2 I + \beta_1\left(\bar{F}_2^{(j)}\right)^H\bar{F}_2^{(j)}\right]^{-1}\bar{C}_2^{(j,t+1)}\left(\hat{Y}_2^{(j,t)}\right)^H\left[\hat{Y}_2^{(j,t)}\left(\hat{Y}_2^{(j,t)}\right)^H + \lambda I\right]^{-1}, \tag{14}$$

$$\begin{aligned}\hat{Y}_2^{(j,t+1)} &= \left[\alpha_2\left(\hat{X}_2^{(j,t+1)}\right)^H\hat{X}_2^{(j,t+1)} + \beta_1\left(\bar{F}_2^{(j)}\hat{X}_2^{(j,t+1)}\right)^H\bar{F}_2^{(j)}\hat{X}_2^{(j,t+1)} + \lambda I\right]^{-1} \\ &\quad \alpha_2\left(\hat{X}_2^{(j,t+1)}\right)^H\bar{C}_2^{(j,t+1)},\end{aligned} \tag{15}$$

$$\begin{aligned}\hat{X}_3^{(k,t+1)} &= \alpha_3\bar{C}_3^{(k,t+1)}\left(\hat{Y}_3^{(k,t)}\right)^H \\ &\quad \left[\alpha_3\hat{Y}_3^{(k,t)}\left(\hat{Y}_3^{(k,t)}\right)^H + \beta_2\left(\hat{Y}_3^{(k,t)}\bar{G}_3^{(k)}\right)\left(\hat{Y}_3^{(k,t)}\bar{G}_3^{(k)}\right)^H + \lambda I\right]^{-1},\end{aligned} \tag{16}$$

and

$$\begin{aligned}\hat{Y}_3^{(k,t+1)} &= \alpha_3\left[\left(\hat{X}_3^{(k,t+1)}\right)^H\hat{X}_3^{(k,t+1)} + \lambda I\right]^{-1}\left(\hat{X}_3^{(k,t+1)}\right)^H\bar{C}_3^{(k,t+1)} \\ &\quad \left[\alpha_3 I + \beta_2\bar{G}_3^{(k)}\left(\bar{G}_3^{(k)}\right)^H\right]^{-1}.\end{aligned} \tag{17}$$

Based on above analysis, the alternating minimization method can be outlined as Algorithm 3.1, denoted by STTF for convenience.

Remark 1 In general, we do not know the true tensor fibered rank of optimal tensor $\mathcal{C}$ in advance. Thus, it is necessary to estimate the tensor fibered rank of tensor $\mathcal{C}$. In this paper, we adopt the same rank estimation and rank decreasing strategy proposed in [38, 40, 48]. Similar to [38, 40], we adopt the rank decreasing method to estimate the true rank of a tensor. For the ease of the reader, we present the strategy here. Suppose that the tensor fibered rank of $\mathcal{C}$ is $\left(r_1^t, r_2^t, r_3^t\right)$ with $r_u^t = \max\left\{r_u^{1,t}, r_u^{2,t}, \ldots, r_u^{n_u,t}\right\}$ and $r_u^{l,t} := \text{rank}\left(\bar{C}_u^{(l,t)}\right)$ for $u \in [\mathbf{3}]$ and $l \in [\boldsymbol{n_u}]$ at the tth iteration. We compute the eigenvalues of $\left(\hat{X}_u^{(l)}\right)^H\hat{X}_u^{(l)}$ and then sort all

Algorithm 3.1 Tensor Factorization for Tensor Completion with Spatio-temporal Characterization (STTF)

Input: The tensor data $\mathcal{M} \in \mathbb{C}^{n_1 \times n_2 \times n_3}$, $\mathcal{F}$, $\mathcal{G}$, $\mathcal{H}$, the observed set Ω, the initialized rank R^0, parameters λ, ε, α_u and β_u, $u \in [\mathbf{3}]$.
Initialization: $\mathcal{X}_u^0$, $\mathcal{Y}_u^0$, $u \in [\mathbf{3}]$.
While not converge do
1. Fix $\hat{X}_u^t$ and $\hat{Y}_u^t$, compute $\mathcal{C}^{t+1}$ by (11).
2. Compute $\hat{X}_u^{t+1}$ by (12), (14) and (16) by fixing $\hat{Y}_u^t$ and $\mathcal{C}^{t+1}$.
3. Obtain $\hat{Y}_u^{t+1}$ by (13), (15) and (17) based on $\hat{X}_u^{t+1}$ and $\mathcal{C}^{t+1}$.
4. Adopt the rank decreasing scheme to adjust rank$_f(\mathcal{A})$ and the sizes of $\hat{X}_u^{t+1}$ and $\hat{Y}_u^{t+1}$.
5. Check the stop criterion $\left\|\mathcal{C}^{t+1} - \mathcal{C}^t\right\|_F^2 / \|\mathcal{C}^t\|_F^2 < \varepsilon$.
6. $t \leftarrow t + 1$.
end while
Output: $\mathcal{C}^{t+1}$.

these eigenvalues for each u, and we can obtain $\lambda_u^1 \geqslant \lambda_u^2 \geqslant \cdots \geqslant \lambda_u^{n_u^t}$ with $n_u^t = \sum_{l=1}^{n_u} r_u^{l,t}$. Finally, we compute the quotients $\hat{\lambda}_u^z = \lambda_u^z / \lambda_u^{z+1}$ for $z \in [\boldsymbol{n_u^t - 1}]$. Compute $\tau_u^t = \left(T_u^t - 1\right) \hat{\lambda}_u^{T_u^t} / \sum_{z \neq T_u^t} \hat{\lambda}_u^z$ with $T_u^t = \arg\max_{1 \leqslant z \leqslant n_u^t - 1} \hat{\lambda}_u^z$. If $\tau_u^t \geqslant 10$ (there being a large drop in the magnitude of the eigenvalues), we should reduce r_u^t. We find $\lambda_u^{s_u^t}$ such that it meets $\sum_{l=1}^{s_u^t} \lambda_u^l / \sum_{l=1}^{n_u} \lambda_u^l \geqslant 95\%$. Assume there are $m_u^{l,t}$ eigenvalues of $\left(\hat{X}_u^{(l,t)}\right)^H \hat{X}_u^{(l,t)}$ which belong to $\left\{\lambda_u^{s_u^t+1}, \ldots, \lambda_u^{n_u}\right\}$. Then we set $r_u^{l,t} = r_u^{l,t} - m_u^{l,t}$. Suppose $U_u^{(l)} \Sigma_u^{(l)} \left(V_u^{(l)}\right)^H$ is the skinny SVD of $\hat{X}_u^{(l)} \hat{Y}_u^{(l)}$. We can update $\hat{X}_u^{(l)} = U^{(l)}_{u,r_u^{l,t}} \Sigma^{(l)}_{u,r_u^{l,t}}$ and $\hat{Y}_u^{(l)} = \left(V^{(l)}_{u,r_u^{l,t}}\right)^H$, where

- $U^{(l)}_{u,r_u^{l,t}}$ consists of the first $r_u^{l,t}$ columns of $U_u^{(l)}$;
- $\Sigma^{(l)}_{u,r_u^{l,t}}$ is a diagonal matrix whose diagonal entries are the largest $r_u^{l,t}$ eigenvalues of $\Sigma_u^{(l)}$;
- $V^{(l)}_{u,r_u^{l,t}}$ consists of the first $r_u^{l,t}$ rows of $V_u^{(l)}$.

In this way, we can adjust the rank r_u^t for $u \in [\mathbf{3}]$ and estimate the true rank of the tensor data.

3.2 Convergence Analysis

In this subsection, we present the convergence of STTF. The following notation will be used in our analysis. In problem (8), Ω is an index set which locates the observed data. We use Ω^c to denote the complement of the set Ω with respect to the set $\{(i, j, k) : i \in [\mathbf{n_1}], j \in [\mathbf{n_2}], k \in [\mathbf{n_3}]\}$. To simply the notation, we denote $z^t = \left(\mathcal{C}^t, \mathcal{X}_1^t, \mathcal{X}_2^t, \mathcal{X}_3^t, \mathcal{Y}_1^t, \mathcal{Y}_2^t, \mathcal{Y}_3^t\right)$ in this subsection. Furthermore, we denote

$$
\begin{aligned}
g^t(\mathcal{C}) &= \sum_{u=1}^{3} \frac{\alpha_u}{2} \left\| \mathcal{X}_u^t *_u \mathcal{Y}_u^t - \mathcal{C} \right\|_F^2, \\
p_1^t(\mathcal{X}_1) &= \frac{\alpha_1}{2} \left\| \mathcal{X}_1 *_1 \mathcal{Y}_1^t - \mathcal{C}^{t+1} \right\|_F^2 + \frac{\beta_3}{2} \left\| \left(\mathcal{X}_1 *_1 \mathcal{Y}_1^t \right) *_1 \mathcal{H} \right\|_F^2 + \frac{\lambda}{2} \| \mathcal{X}_1 \|_F^2, \\
p_2^t(\mathcal{X}_2) &= \frac{\alpha_2}{2} \left\| \mathcal{X}_2 *_2 \mathcal{Y}_2^t - \mathcal{C}^{t+1} \right\|_F^2 + \frac{\beta_1}{2} \left\| \mathcal{F} *_2 \left(\mathcal{X}_2 *_2 \mathcal{Y}_2^t \right) \right\|_F^2 \\
&\quad + \frac{\lambda}{2} \left(\beta_1 \| \mathcal{F} *_2 \mathcal{X}_2 \|_F^2 + \alpha_2 \| \mathcal{X}_2 \|_F^2 \right), \\
p_3^t(\mathcal{X}_3) &= \frac{\alpha_3}{2} \left\| \mathcal{X}_3 *_3 \mathcal{Y}_3^t - \mathcal{C}^{t+1} \right\|_F^2 + \frac{\beta_2}{2} \left\| \left(\mathcal{X}_3 *_3 \mathcal{Y}_3^t \right) *_3 \mathcal{G} \right\|_F^2 + \frac{\lambda}{2} \| \mathcal{X}_3 \|_F^2, \\
q_1^t(\mathcal{Y}_1) &= \frac{\alpha_1}{2} \left\| \mathcal{X}_1^{t+1} *_1 \mathcal{Y}_1 - \mathcal{C}^{t+1} \right\|_F^2 + \frac{\beta_3}{2} \left\| \left(\mathcal{X}_1^{t+1} *_1 \mathcal{Y}_1 \right) *_1 \mathcal{H} \right\|_F^2 \\
&\quad + \frac{\lambda}{2} \left(\beta_3 \| \mathcal{Y}_1 *_1 \mathcal{H} \|_F^2 + \alpha_1 \| \mathcal{Y}_1 \|_F^2 \right), \\
q_2^t(\mathcal{Y}_2) &= \frac{\alpha_2}{2} \left\| \mathcal{X}_2^{t+1} *_2 \mathcal{Y}_2 - \mathcal{C}^{t+1} \right\|_F^2 \\
&\quad + \frac{\beta_1}{2} \left\| \mathcal{F} *_2 \left(\mathcal{X}_2^{t+1} *_2 \mathcal{Y}_2 \right) \right\|_F^2 + \frac{\lambda}{2} \| \mathcal{Y}_2 \|_F^2, \\
q_3^t(\mathcal{Y}_3) &= \frac{\alpha_3}{2} \left\| \mathcal{X}_3^{t+1} *_3 \mathcal{Y}_3 - \mathcal{C}^{t+1} \right\|_F^2 + \frac{\beta_2}{2} \left\| \left(\mathcal{X}_3^{t+1} *_3 \mathcal{Y}_3 \right) *_3 \mathcal{G} \right\|_F^2 \\
&\quad + \frac{\lambda}{2} \left(\beta_2 \| \mathcal{Y}_3 *_3 \mathcal{G} \|_F^2 + \alpha_3 \| \mathcal{Y}_3 \|_F^2 \right).
\end{aligned}
$$

Before proceeding, we present the Kurdyka–Lojasiewicz (KL) property [3] with constraint defined as below.

Definition 3 *(Kurdyka–Lojasiewicz (KL) property)* Let Z be an open set and $f : Z \to \mathbb{R}$ be a semi-algebraic function. For every critical point $z^\star \in Z$ of f, there are a neighborhood of $z^\star$, denoted by $Z' \subset Z$, an exponent $\theta \in [0, 1)$ and a positive constant μ such that

$$
|f(z) - f(z^\star)|^\theta \leq \mu \left\| \prod_\Omega (\nabla f(z)) \right\|_F, \tag{18}
$$

where

$$
\begin{aligned}
&\prod_\Omega (\nabla f(z)) = (P_\Omega (\nabla_{\mathcal{C}} f(z)); \\
&\nabla_{\mathcal{X}_1} f(z); \nabla_{\mathcal{X}_2} f(z); \nabla_{\mathcal{X}_3} f(z); \nabla_{\mathcal{Y}_1} f(z); \nabla_{\mathcal{Y}_2} f(z); \nabla_{\mathcal{Y}_3} f(z)).
\end{aligned}
$$

Note that $f(z)$, defined as in (9), is a quadratic function on z, and hence is a semi-algebraic function. From Definition 3, for any critical point $z^\star$, there exist θ and μ such that (18) is satisfied.

Theorem 1 *Suppose that $\{z^t\}$ is an infinite sequence generated by STTF. Then we have the following statements:*

(1) *the sequence* $\{z^t\}$ *is bounded and any accumulation point of* $\{z^t\}$ *is a stationary point of problem* (9)*;*
(2) *there is a constant* $\eta > 0$ *such that* $\eta\|z^t - z^{t+1}\|_F \geq \|\prod_{\Omega}(\nabla f(z^t))\|_F$.

Proof Since rank $r \geq 0$ in STTF is non-increasing, we can assume that the rank r is fixed for all z^t when t is sufficiently large. That is, the rank decreasing scheme is not adopted for all such big enough t. For simplicity, we assume that t is big enough such that r is fixed and denote $f^t = f(z^t)$ in the following.

(1) By (11), it follows

$$\begin{aligned}\|\mathcal{C}^{t+1} - \mathcal{C}^t\|_F^2 &= \left\|\sum_{u=1}^{3}\alpha_u\mathcal{X}_u^t *_u \mathcal{Y}_u^t + P_{\Omega}\left(\mathcal{M} - \sum_{u=1}^{3}\alpha_u\mathcal{X}_u^t *_u \mathcal{Y}_u^t\right) - \mathcal{C}^t\right\|_F^2 \\ &= \left\|\sum_{u=1}^{3}\alpha_u\mathcal{X}_u^t *_u \mathcal{Y}_u^t - \mathcal{C}^t + P_{\Omega}\left(\mathcal{M} - \sum_{u=1}^{3}\alpha_u\mathcal{X}_u^t *_u \mathcal{Y}_u^t\right)\right\|_F^2 \\ &= \left\|\left(\sum_{u=1}^{3}\alpha_u\mathcal{X}_u^t *_u \mathcal{Y}_u^t - \mathcal{C}^t\right)_{\Omega^c}\right\|_F^2.\end{aligned}$$

According to STTF, we have that

$$\begin{aligned}f^t - f^{t+1} &= g^t(\mathcal{C}^t) - g^t(\mathcal{C}^{t+1}) + \sum_{u=1}^{3}\left(p_u^t(\mathcal{X}_u^t) - p_u^t(\mathcal{X}_u^{t+1})\right) + \sum_{u=1}^{3}\left(q_u^t(\mathcal{Y}_u^t) - q_u^t(\mathcal{Y}_u^{t+1})\right) \\ &\geqslant \frac{1}{2}\left(\left\|\sum_{u=1}^{3}\alpha_u\mathcal{X}_u^t *_u \mathcal{Y}_u^t - \mathcal{C}^t\right\|_F^2 - \left\|\sum_{u=1}^{3}\alpha_u\mathcal{X}_u^t *_u \mathcal{Y}_u^t - \mathcal{C}^{t+1}\right\|_F^2\right) \\ &\quad + \sum_{u=1}^{3}\sum_{l=1}^{n_u}\frac{\zeta}{2n_u}\left(\left\|\hat{X}_u^{(l,t)} - \hat{X}_u^{(l,t+1)}\right\|_F^2 + \left\|\hat{Y}_u^{(l,t)} - \hat{Y}_u^{(l,t+1)}\right\|_F^2\right) \\ &= \frac{1}{2}\left\|\left(\sum_{u=1}^{3}\alpha_u\mathcal{X}_u^t *_u \mathcal{Y}_u^t - \mathcal{C}^t\right)_{\Omega^c}\right\|_F^2 + \frac{\zeta}{2}\sum_{u=1}^{3}\left(\|\mathcal{X}_u^t - \mathcal{X}_u^{t+1}\|_F^2 + \|\mathcal{Y}_u^t - \mathcal{Y}_u^{t+1}\|_F^2\right) \\ &= \frac{1}{2}\|\mathcal{C}^{t+1} - \mathcal{C}^t\|_F^2 + \frac{\zeta}{2}\sum_{u=1}^{3}\left(\|\mathcal{X}_u^t - \mathcal{X}_u^{t+1}\|_F^2 + \|\mathcal{Y}_u^t - \mathcal{Y}_u^{t+1}\|_F^2\right) \\ &\geq \frac{\min\{1,\zeta\}}{2}\|z^{t+1} - z^t\|_F^2,\end{aligned} \tag{19}$$

where $\zeta = \lambda\min\{1, \alpha_1, \alpha_2, \alpha_3\}$ and the first inequality holds from the property of strongly convex functions. Therefore, $\{f^t\}$ is monotonically decreasing. Together with the fact that $f \geq 0$, the series $\sum_{t=1}^{\infty}\left(f^t - f^{t+1}\right) = f^1 - \lim_{t\to\infty} f^t$ converges. Hence,

$$\sum_{t=1}^{\infty}\left(f^t - f^{t+1}\right) < \infty, \quad \sum_{t=1}^{\infty}\left\|z^t - z^{t+1}\right\|_F^2 < \infty.$$

Since $f^t \geqslant \frac{\zeta}{2}\sum_{u=1}^{3}\left(\left\|\mathcal{X}_u^t\right\|_F^2+\left\|\mathcal{Y}_u^t\right\|_F^2\right)$, $\{\mathcal{X}_u^t\}$ and $\{\mathcal{Y}_u^t\}$ are bounded. Together with the expression of $\mathcal{C}^t$, it is asserted that $\{\mathcal{C}^t\}$ is also bounded, and hence $\{z^t\}$ is bounded.

Clearly, there exists a convergent subsequence of $\{z^t\}$. Without loss of generality, we assume that $\lim_{k\to\infty} z^{t_k}=z^\star$. From $\sum_{t=1}^{\infty}\|z^t-z^{t+1}\|_F^2<\infty$, $\lim_{t\to\infty} z^{t+1}-z^t=0$, and hence $\lim_{k\to\infty} z^{t_k+1}=z^\star$.

Together with (11)–(17), we have that

$$
\begin{aligned}
&\alpha_1\left(\hat{X}_1^\star\hat{Y}_1^\star-\bar{C}_1^\star\right)\left(\hat{Y}_1^\star\right)^H+\lambda\hat{X}_1^\star+\beta_3\hat{X}_1^\star\left(\hat{Y}_1^\star\bar{H}_1\right)\left(\hat{Y}_1^\star\bar{H}_1\right)^H=0,\\
&\alpha_2\left(\hat{X}_2^\star\hat{Y}_2^\star-\bar{C}_2^\star\right)\left(\hat{Y}_2^\star\right)^H+\lambda\alpha_2\hat{X}_2^\star+\lambda\beta_1\bar{F}_2^H\bar{F}_2\hat{X}_2^\star+\beta_1\bar{F}_2^H\bar{F}_2\hat{X}_2^\star\hat{Y}_2^\star\left(\hat{Y}_2^\star\right)^H=0,\\
&\alpha_3\left(\hat{X}_3^\star\hat{Y}_3^\star-\bar{C}_3^\star\right)\left(\hat{Y}_3^\star\right)^H+\lambda\hat{X}_3^\star+\beta_2\hat{X}_3^\star\left(\hat{Y}_3^\star\bar{G}_3\right)\left(\hat{Y}_3^\star\bar{G}_3\right)^H=0,\\
&\alpha_1\left(\hat{X}_1^\star\right)^H\left(\hat{X}_1^\star\hat{Y}_1^\star-\bar{C}_1^\star\right)+\lambda\alpha_1\hat{Y}_1^\star+\lambda\beta_3\hat{Y}_1^\star\bar{H}_1\bar{H}_1^H+\beta_3\left(\hat{X}_1^\star\right)^H\hat{X}_1^\star\hat{Y}_1^\star\bar{H}_1\bar{H}_1^H=0,\\
&\alpha_2\left(\hat{X}_2^\star\right)^H\left(\hat{X}_2^\star\hat{Y}_2^\star-\bar{C}_2^\star\right)+\lambda\hat{Y}_2^\star+\beta_1\left(\bar{F}_2\hat{X}_2^\star\right)^H\left(\bar{F}_2\hat{X}_2^\star\right)\hat{Y}_2^\star=0,\\
&\alpha_3\left(\hat{X}_3^\star\right)^H\left(\hat{X}_3^\star\hat{Y}_3^\star-\bar{C}_3^\star\right)+\lambda\alpha_3\hat{Y}_3^\star+\lambda\beta_2\hat{Y}_3^\star\bar{G}_3\bar{G}_3^H+\beta_2\left(\hat{X}_3^\star\right)^H\hat{X}_3^\star\hat{Y}_3^\star\bar{G}_3\bar{G}_3^H=0,\\
&P_{\Omega}\left(\mathcal{C}^\star-\mathcal{M}\right)=0,\\
&P_{\Omega^c}\left(\sum_{u=1}^{3}\alpha_u\mathcal{X}_u^\star *_u\mathcal{Y}_u^\star-\mathcal{C}^\star\right)=0.
\end{aligned}
$$

Therefore, $z^\star$ is a stationary point of problem (9).

(2) Since $\{z^t\}$ is bounded, there exists a compact convex set Z such that $\{z^t\}\subset Z$. Since f is a quadratic polynomial in z, the gradient ∇f is Lipschitz in Z with a Lipschitz constant L_f, that is,

$$
\|\nabla f(z)-\nabla f(z')\|_F\leq L_f\|z-z'\|_F,\quad \forall\, z,z'\in Z.
$$

Clearly,

$$
\begin{aligned}
\left\|\prod_{\Omega}\left(\nabla_{\mathcal{C}}f\left(z^{t+1}\right)\right)\right\|_F &\leq \left\|\prod_{\Omega}\left(\nabla_{\mathcal{C}}f\left(\mathcal{C}^{t+1},\mathcal{X}_1^{t+1},\ldots,\mathcal{Y}_3^{t+1}\right)\right)\right.\\
&\quad\left.-\prod_{\Omega}\left(\nabla_{\mathcal{C}}f\left(\mathcal{C}^{t},\mathcal{X}_1^{t},\ldots,\mathcal{Y}_3^{t}\right)\right)\right\|_F\\
&\quad+\left\|\prod_{\Omega}\left(\nabla_{\mathcal{C}}f\left(\mathcal{C}^{t},\mathcal{X}_1^{t},\ldots,\mathcal{Y}_3^{t}\right)\right)\right\|_F\\
&\leq L_f\left\|z^{t+1}-z^t\right\|_F+\left\|\left(\mathcal{C}^t-\sum_{u=1}^{3}\alpha_u\mathcal{X}_u^t *_u\mathcal{Y}_u^t\right)_{\Omega^c}\right\|_F\\
&=L_f\left\|z^{t+1}-z^t\right\|_F+\left\|\mathcal{C}^{t+1}-\mathcal{C}^t\right\|_F\\
&\leq\left(L_f+1\right)\left\|z^{t+1}-z^t\right\|_F.
\end{aligned}
$$

Furthermore,

$$
\begin{aligned}
\left\|\nabla_{\mathcal{X}_1}f\left(z^{t+1}\right)\right\|_F &\leq \left\|\nabla_{\mathcal{X}_1}f\left(\mathcal{C}^{t+1},\mathcal{X}_1^{t+1},\ldots,\mathcal{Y}_3^{t+1}\right)-\nabla_{\mathcal{X}_1}f\left(\mathcal{C}^{t+1},\mathcal{X}_1^{t+1},\ldots,\mathcal{Y}_3^{t}\right)\right\|_F\\
&\quad+\left\|\nabla_{\mathcal{X}_1}f\left(\mathcal{C}^{t+1},\mathcal{X}_1^{t+1},\ldots,\mathcal{Y}_3^{t}\right)\right\|_F
\end{aligned}
$$

$$\leq L_f \|z^{t+1} - z^t\|_F + \lambda \|\mathcal{X}_u^{t+1} - \mathcal{X}_u^t\|_F$$
$$\leq \left(L_f + \lambda\right) \left\|z^{t+1} - z^t\right\|_F .$$

Similarly, for any $u \in [\mathbf{3}]$, we have

$$\left\|\nabla_{\mathcal{X}_u} f(z^{t+1})\right\|_F \leq \left(L_f + \lambda\right) \left\|z^{t+1} - z^t\right\|_F ,$$
$$\left\|\nabla_{\mathcal{Y}_u} f(z^{t+1})\right\|_F \leq \left(L_f + \lambda\right) \left\|z^{t+1} - z^t\right\|_F .$$

Now we can assert that $\| \prod_{\Omega} \left(\nabla f(z^{t+1})\right) \|_F \leq (7L_f + 6\lambda + 1)\|z^{t+1} - z^t\|_F$ and the result (2) is arrived with $\eta := 7L_f + 6\lambda + 1$. □

Theorem 2 *Suppose that $z^\star$ is an accumulation point of $\{z^t\}$ generated by STTF. Assume that the starting point z^0 satisfies $z^0 \in B(z^\star, \sigma) := \{z : \|z - z^\star\|_F < \sigma\} \subseteq Z'$, θ and μ are defined as in Definition 3. Suppose that $\rho = \frac{\min\{1,\lambda\}}{2\eta}$ with η and λ being from Theorem 1 (2) and*

$$\sigma > \frac{\mu}{\rho(1-\theta)} \left| f\left(z^0\right) - f\left(z^\star\right)\right|^{1-\theta} + \left\|z^0 - z^\star\right\|_F .$$

Then

(1) $z^t \in B(z^\star, \sigma)$, *for* $t = 0, 1, 2, \ldots$;
(2) $\sum_{t=0}^{\infty} \left\|z^{t+1} - z^t\right\|_F \leq \frac{\mu}{\rho(1-\theta)} \left| f\left(z^0\right) - f\left(z^\star\right)\right|^{1-\theta}$;
(3) $\lim_{t\to\infty} z^t = z^\star$.

Proof We show (1) by induction. Clearly, (1) is true for $t = 0$ by assumption. Assume that (1) holds for all $t \leq \bar{t}$, then KL property holds for such z^t. Now we show that (1) is true for $t = \bar{t} + 1$.

Let $\theta \in (0, 1)$ and $\phi(s) := \frac{\mu}{(1-\theta)} \left(s - f(z^\star)\right)^{1-\theta}$, $s \geq f(z^\star)$. Then, $\phi(s)$ is concave with its derivative $\phi'(s) = \frac{\mu}{|s - f(z^\star)|^\theta}$ for $s > f(z^\star)$. Since $\phi(s)$ is concave, we have

$$\phi\left(f\left(z^t\right)\right) - \phi\left(f\left(z^{t+1}\right)\right) \geq \phi'\left(f\left(z^t\right)\right)\left[f\left(z^t\right) - f\left(z^{t+1}\right)\right]$$
$$= \frac{\mu}{\left|f\left(z^t\right) - f\left(z^\star\right)\right|^\theta}\left[f\left(z^t\right) - f\left(z^{t+1}\right)\right].$$

Combining with (18) (19) and Theorem 1 (2), we have

$$\phi\left(f\left(z^t\right)\right) - \phi\left(f\left(z^{t+1}\right)\right) \geq \frac{1}{\left\|\prod_{\Omega}\left(\nabla f(z^t)\right)\right\|_F}\left[f\left(z^t\right) - f\left(z^{t+1}\right)\right] \geq \rho \left\|z^{t+1} - z^t\right\|_F .$$

Hence,

$$\begin{aligned}\sum_{p=0}^{t}\left\|z^{k+1}-z^{k}\right\|_F &\leq \frac{1}{\rho}\sum_{p=0}^{t}\left[\phi\left(f\left(z^{t}\right)\right)-\phi\left(f\left(z^{t+1}\right)\right)\right]\\ &=\frac{1}{\rho}\left[\phi\left(f\left(z^{0}\right)\right)-\phi\left(f\left(z^{t+1}\right)\right)\right]\\ &\leq \frac{1}{\rho}\phi\left(f\left(z^{0}\right)\right).\end{aligned} \tag{20}$$

This implies that

$$\left\|z^{t+1}-z^{\star}\right\|_F \leq \sum_{p=0}^{t}\left\|z_{t+1}-z_t\right\|_F+\left\|z^{0}-z^{\star}\right\|_F \leq \frac{1}{\rho}\phi\left(f\left(z^{0}\right)\right)+\left\|z^{0}-z^{\star}\right\|_F<\sigma.$$

Then we have $z^{t+1}\in B\left(z^{\star},\sigma\right)$, and hence (1) is asserted.

(2) Taking $t\to\infty$ in (20), (2) is arrived.

(3) From (2), for any $\epsilon>0$, there exists $K_1>0$ such that for any $t\geq K_1$ such that $\|z^{t}-z^{t_k}\|_F\leq\sum_{i=1}^{t_k-t}\|z^{t+i}-z^{t+i-1}\|_F<\frac{\epsilon}{2}$. From $\lim_{k\to\infty}z^{t_k}=z^{\star}$, there exists $K_2>0$ such that for all $k>K_2$, $\|z^{t_k}-z^{\star}\|_F<\frac{\epsilon}{2}$. Hence, for any $t\geq\max\{K_1,K_2\}$,

$$\|z^{t}-z^{\star}\|_F\leq\|z^{t}-z^{t_k}\|_F+\|z^{t_k}-z^{\star}\|_F\leq\epsilon,$$

which indicates that $z^{t}\to z^{\star}$. □

Theorem 3 *Suppose that $\left\{z^{t}\right\}$ is an infinite sequence generated by STTF with an accumulating point $z^{\star}$ and θ, μ are as in Definition 3. Then*

(a) If $\theta\in\left(0,\frac{1}{2}\right]$, then there exist $\gamma>0$ and $c\in(0,1)$ such that $\left\|z^{t}-z^{\star}\right\|_F\leq\gamma c^{t}$;

(b) If $\theta\in\left(\frac{1}{2},1\right)$, then there exists $\gamma>0$ such that $\left\|z^{t}-z^{\star}\right\|_F\leq\gamma t^{-\frac{1-\theta}{2\theta-1}}$.

Proof Assume that $z^{0}\in B\left(z^{\star},\sigma\right)$. Denote that $\Delta_t:=\sum_{p=t}^{\infty}\left\|z^{p}-z^{p+1}\right\|_F$. Then

$$\left\|z^{t}-z^{\star}\right\|_F\leq\Delta_t. \tag{21}$$

From Theorem 2 (2), we have

$$\Delta_t\leq\frac{\mu}{\rho(1-\theta)}\left|f\left(z^{0}\right)-f\left(z^{\star}\right)\right|^{1-\theta}=\frac{\mu}{\rho(1-\theta)}\left[\left|f\left(z^{0}\right)-f\left(z^{\star}\right)\right|^{\theta}\right]^{\frac{1-\theta}{\theta}}.$$

Combining with the KL inequality, there holds

$$\Delta_t\leq\frac{\mu}{\rho(1-\theta)}\left(\mu\left\|\prod\nolimits_{\Omega}(\nabla f(z))\right\|_F\right)^{\frac{1-\theta}{\theta}}.$$

From Theorem 1 (2), the above inequality implies that

$$\Delta_t\leq\frac{\mu}{\rho(1-\theta)}\left(\mu\eta\left\|z^{t}-z^{t+1}\right\|_F\right)^{\frac{1-\theta}{\theta}}=c_1\left(\Delta_t-\Delta_{t+1}\right)^{\frac{1-\theta}{\theta}}. \tag{22}$$

where $c_1 = \frac{\mu}{\rho(1-\theta)}(\mu\eta)^{\frac{1-\theta}{\theta}}$ is a positive constant.

(a) If $\theta \in \left(0, \frac{1}{2}\right]$, then $\frac{1-\theta}{\theta} \geq 1$. For sufficiently large t, it holds $\Delta_t \leq c_1(\Delta_t - \Delta_{t+1})$. Hence $\Delta_{t+1} \leq \frac{c_1-1}{c_1}\Delta_t$. Together with (21), result (a) is arrived with $c = \frac{c_1-1}{c_1}$.

(b) For case of $\theta \in \left(\frac{1}{2}, 1\right)$, let $h(s) = s^{-\frac{\theta}{1-\theta}}$. The function $h(s)$ is monotonically decreasing on s. By (22), we have

$$\begin{aligned} c_1^{-\frac{\theta}{1-\theta}} &\leq h(\Delta_t)(\Delta_t - \Delta_{t+1}) = \int_{\Delta_{t+1}}^{\Delta_t} h(\Delta_t)\,ds \leq \int_{\Delta_{t+1}}^{\Delta_t} h(s)ds \\ &= -\frac{1-\theta}{2\theta-1}\left(\Delta_t^{-\frac{2\theta-1}{1-\theta}} - \Delta_{t+1}^{-\frac{2\theta-1}{1-\theta}}\right). \end{aligned}$$

Since $\theta \in \left(\frac{1}{2}, 1\right)$, $\nu := -\frac{2\theta-1}{1-\theta} < 0$ and $\Delta_{t+1}^{\nu} - \Delta_t^{\nu} \geq -\nu c_1^{-\frac{\theta}{1-\theta}} > 0$. Thus, there is a $\hat{t}$ such that for all $t \geq 2\hat{t}$,

$$\Delta_t^{\nu} \geq \Delta_{\hat{t}}^{\nu} - \nu c_1^{-\frac{\theta}{1-\theta}}(t - \hat{t}) \geq -\nu c_1^{-\frac{\theta}{1-\theta}}(t - \hat{t}) \geq -\frac{\nu}{2}c_1^{-\frac{\theta}{1-\theta}}t,$$

then we have $\Delta_t \leq \gamma t^{\frac{1}{\nu}}$ for a certain positive constant $\gamma = \left(-\frac{\nu}{2}c_1^{-\frac{\theta}{1-\theta}}\right)^{\frac{1}{\nu}}$. Then result (b) is obtained. □

4 Numerical Experiments

In this section, we report some numerical results of our proposed STTF to show its validity. We employ the peak signal-to-noise ratio (PSNR), the structural similarity (SSIM) [37], and the feature similarity (FSIM) [43] to measure the quality of the recovered results. We conduct extensive experiments to evaluate our method, and then compare the results with those by some other existing methods, including WSTNN [46], CTNN [44], TNN [45], TCTF [48], TMac [40], NTD [39] and NCPC [41]. All the methods are implemented on the platform of Windows 10 and Matlab (R2020b) with an Intel(R) Core(TM) i5-12500H CPU at 2.50GHz and 16 GB RAM.

Parameter selection In all tests, the maximum number of iterations is set to be 300 and the termination precision ε is set to be 10^{-5}. In STTF, the parameter λ is set as 10^{-4} and F, G, H are all set to Toeplitz matrices. Table 1 shows the parameter settings for the proposed STTF method on different data.

4.1 Color Image Inpainting

In this subsection, we apply our STTF method to the task of color image inpainting. As color images can be expressed as third-order tensors, we model the image inpainting problem as a tensor completion problem, assuming that the tensor data is of low-rank or numerical low-rank. For image inpainting evaluation, we use the Berkeley

Table 1 Parameter settings of STTF on different data

Test		$(\alpha_1, \alpha_2, \alpha_3)$	$(\beta_1, \beta_2, \beta_3)$
Image	SR = 10%	(1,2,3)/6	(0.5,0.1,0)
	SR = 15%		(0.3,0.08,0)
	SR = 20%		(0.1,0.05,0)
Video	SR = 10%	(1,1,1)/3	(0.001,0.01,100)
Internet traffic	SR = 10%	(1,1,1)/3	(0,20,0)
	SR = 20%		(0,2,0)
	SR = 30%		(0,0.8,0)
	SR = 40%		(0,0.6,0)
	SR = 50%		(0,0.4,0)
	SR ≥ 60%		(0,0.05,0)

Table 2 The average PSNR, SSIM, and FSIM values for all 50 images tested by eight methods

SR	10%			15%			20%		
Method	PSNR	SSIM	FSIM	PSNR	SSIM	FSIM	PSNR	SSIM	FSIM
STTF	**27.868**	**0.851**	**0.887**	**30.606**	**0.909**	**0.926**	**31.996**	**0.919**	**0.936**
WSTNN	25.803	0.829	0.861	28.034	0.875	0.895	29.470	0.904	0.915
CTNN	25.603	0.667	0.791	28.010	0.773	0.854	29.943	0.838	0.895
TNN	25.538	0.662	0.788	27.984	0.767	0.850	29.759	0.831	0.889
TCTF	11.549	0.095	0.316	18.305	0.372	0.573	26.062	0.691	0.802
TMac	10.972	0.102	0.331	14.397	0.338	0.536	21.995	0.520	0.691
NTD	24.662	0.555	0.724	26.602	0.674	0.791	27.939	0.749	0.834
NCPC	23.170	0.449	0.662	26.459	0.642	0.779	28.347	0.745	0.836

Bold values indicate the best results

Segmentation database [29] as our test dataset. Our test set consists of 50 images, each of size 481 × 321 × 3. We set the initial tensor fibered rank $(r_u^l)^0 = 3, u \in [\mathbf{2}]$, $(r_3^1)^0 = 50$, $(r_3^2)^0 = \cdots = (r_3^{n_3})^0 = 5$ in STTF, the initial tubal rank (50, 5, 5) in TCTF, the initial Tucker rank (30, 30, 3) in TMac and NTD and the initial CP rank 50 in NCPC.

Table 2 shows the mean values of three metrics (PSNR, SSIM, and FSIM) for all 50 images with different sampling rates (10%, 15%, and 20%). Our STTF method achieves the best image recovery results under all three sampling rates. The higher the sampling rate, the more obvious the advantage of STTF. And when the sampling rate is 10%, STTF outperforms the second best method by 8.00%, 2.65%, and 3.02% in terms of PSNR, SSIM, and FSIM, respectively. A visual comparison of the image inpainting results for "Church" with a 20% sampling rate is shown in Fig. 1. It can be seen that STTF is obviously superior to the comparison methods in the recovery of rich shape structure and texture information.

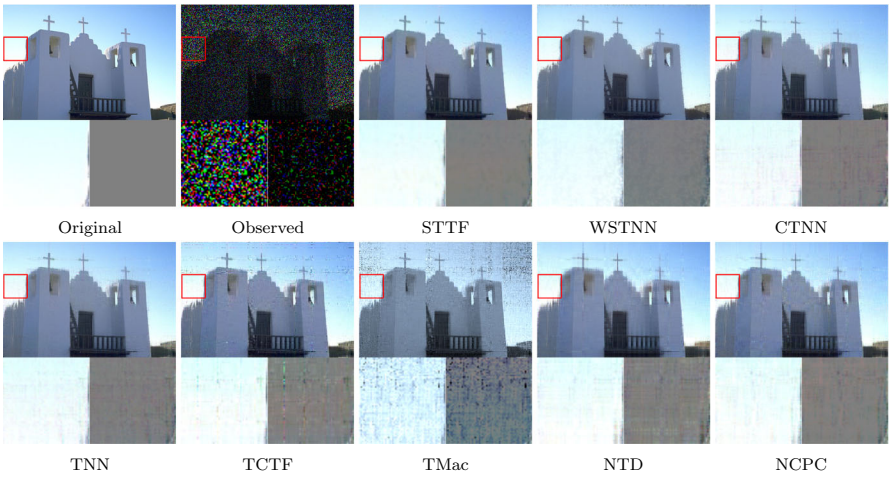

Fig. 1 The completion results of "Church" with SR = 20%

4.2 Video Inpainting

We evaluate our proposed method STTF on the widely used YUV Video Sequences[1] and we pick the first 8 frames. In the experiments, we test our proposed method and other methods on three videos with 144×176 pixels. We test the videos with random missing data of sampling ratio SR $= 10\%$. We set the initial tensor fibered rank $(r_u^l)^0 = 3, u \in [\mathbf{2}]$, $(r_3^1)^0 = 50$, $(r_3^2)^0 = \cdots = (r_3^{n_3})^0 = 10$ in STTF, the initial tubal rank $(10, 1, \ldots, 1)$ in TCTF, the initial Tucker rank $(50, 50, 3)$ in NTD and $(10, 10, 3)$ in TMac, and the initial CP rank 50 in NCPC.

Figure 2 shows the 8th frame of video "Mother". Table 3 presents the numerical results, which show that STTF performs better than other methods. It can be seen that the recovered frame by STTF preserves more details while the competing methods generate undesired artifacts. These results are consistent with those of color image inpainting, further demonstrating the superior performance of our method.

4.3 Internet Traffic Inpainting

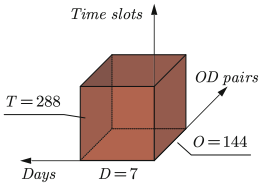

We model the traffic data as a third-order tensor $\mathcal{M} \in \mathbb{R}^{D \times T \times O}$. Here O corresponds to the number of OD pairs with $O = N \times N$ (N is the number of nodes in the network), and there are D days to consider with each day having T time slots.

We use Abilene trace data [34] as an example to illustrate this model. The traffic data consists of measurements between 144 OD pairs every 5 min for 168 days, which corresponds to 288 time slots per day. We use the complete traffic data of one week.

[1] http://trace.eas.asu.edu/yuv/.

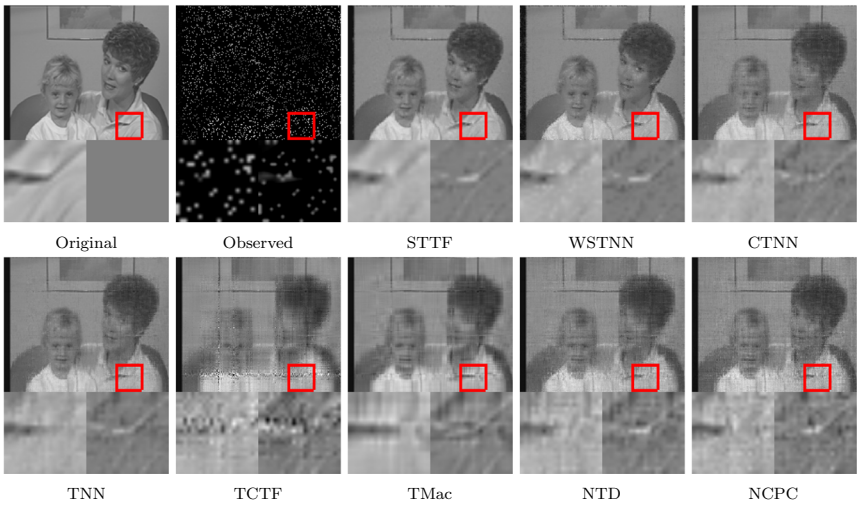

Fig. 2 The completion results at the 8th frame of video "Mother" with SR $= 10\%$

Table 3 The PSNR, SSIM and FSIM values output by eight methods for videos

Video	Container			Mother			Bridge		
Method	PSNR	SSIM	FSIM	PSNR	SSIM	FSIM	PSNR	SSIM	FSIM
STTF	**27.542**	**0.890**	**0.921**	**33.261**	**0.919**	**0.951**	**28.516**	**0.851**	**0.931**
WSTNN	25.503	0.869	0.882	30.172	0.891	0.915	26.964	0.834	0.898
CTNN	24.872	0.795	0.875	30.155	0.828	0.917	26.772	0.773	0.894
TNN	24.724	0.799	0.873	30.095	0.824	0.910	26.656	0.767	0.890
TCTF	20.307	0.617	0.784	24.779	0.598	0.807	22.532	0.525	0.769
TMac	23.417	0.725	0.837	28.153	0.738	0.856	25.478	0.684	0.848
NTD	22.797	0.661	0.806	27.292	0.672	0.845	24.834	0.610	0.812
NCPC	21.809	0.588	0.773	25.453	0.549	0.796	23.040	0.519	0.783

Bold values indicate the best results

Therefore, the trace data can be modeled as a third-order tensor $\mathcal{M} \in \mathbb{R}^{7\times 288\times 144}$. We measure the quality of the recovered data by the normalized mean absolute error (NMAE) in the missing values. The NMAE is defined as follows:

$$\text{NMAE} = \frac{\sum_{(i,j,k)\notin\Omega} \left|\mathcal{M}_{ijk} - \mathcal{C}^{\star}_{ijk}\right|}{\sum_{(i,j,k)\notin\Omega} \left|\mathcal{M}_{ijk}\right|}.$$

Figure 3 shows the recovered results in Abilene dataset by eight algorithms. The X-axis represents the sampling rate of data, and the Y-axis represents NMAE. As the sampling rate increases, the NMAE value gradually decreases except for TMac and TCTF. As shown in Fig. 3, the proposed method STTF significantly outperforms the other methods under various missing rates. This phenomenon implies that the spatio-

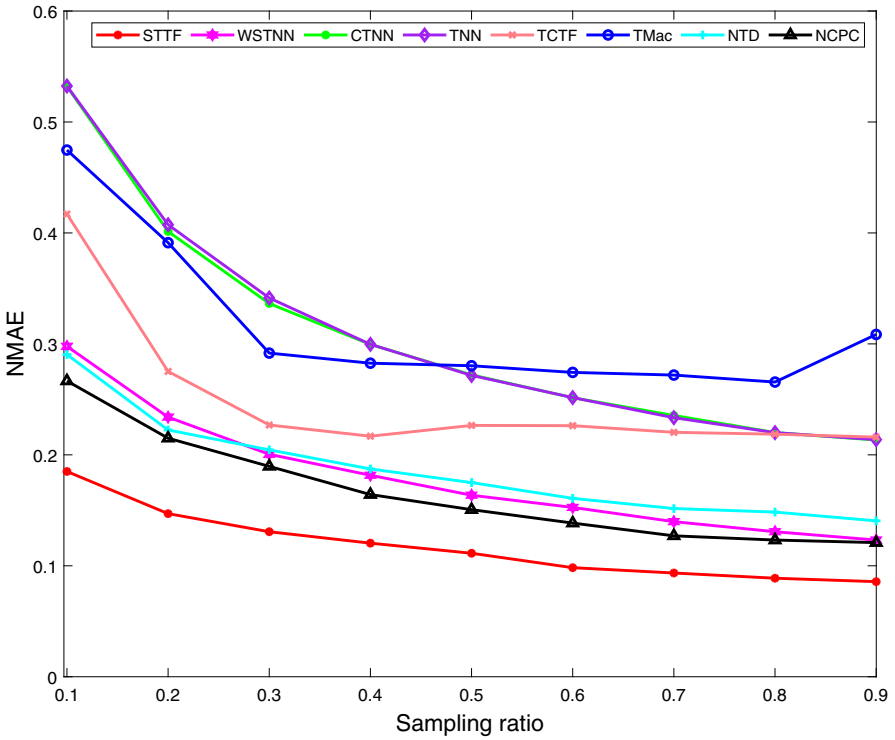

Fig. 3 Comparison on the NMAE by eight methods of different sampling ratios

temporal structure in the internet traffic tensor is valuable and has been exploited to improve the recovery accuracy. Among the eight methods, STTF has the best recovery effect. Note that STTF can still recover missing data with a very low error even if the sampling rate is very low.

5 Conclusion

In this paper, we have presented a novel tensor completion model that incorporates some characteristics of the color image data, the video data and the internet traffic data. By using some constraint matrices to represent these characteristics, our model leveraged the tensor fibered rank to reduce the complexity and improved the accuracy of tensor completion. We have proposed a tensor factorization-based method to solve the optimization problem. Our experimental results on various real-world datasets demonstrated that our method outperformed existing methods in the literature significantly.

Acknowledgements Xinzhen Zhang was partially supported by NSFC (11871369). Zheng-Hai Huang was partially supported by NSFC (12171357).

Data Availability Codes supporting the numerical results are freely available in the GitHub repository, https://github.com/quanyumath/STTF.

References

1. Alderson, D., Chang, H., Roughan, M., Uhlig, S., Willinger, W.: The many facets of internet topology and traffic. Netw. Heterog. Media **1**(4), 569–600 (2006)
2. Asif, M.T., Mitrovic, N., Dauwels, J., Jaillet, P.: Matrix and tensor based methods for missing data estimation in large traffic networks. IEEE Trans. Intell. Transp. Syst. **17**(7), 1816–1825 (2016)
3. Attouch, H., Bolte, J., Svaiter, B.F.: Convergence of descent methods for semi-algebraic and tame problems: proximal algorithms, forward-backward splitting, and regularized Gauss-Seidel methods. Math. Program. **137**(1–2), 91–129 (2013)
4. Bai, M., Zhang, X., Ni, G., Cui, C.: An adaptive correction approach for tensor completion. SIAM J. Imaging Sci. **9**(3), 1298–1323 (2016)
5. Bengua, J.A., Phien, H.N., Tuan, H.D., Do, M.N.: Efficient tensor completion for color image and video recovery: low-rank tensor train. IEEE Trans. Image Process. **26**(5), 2466–2479 (2017)
6. Booth, D.E.: Multi-way analysis: applications in the chemical sciences. Technometrics **47**(4), 518–519 (2005)
7. Carroll, J.D., Chang, J.J.: Analysis of individual differences in multidimensional scaling via an n-way generalization of "Eckart-Young" decomposition. Psychometrika **35**(3), 283–319 (1970)
8. Chang, J., Chen, Y., Qi, L., Yan, H.: Hypergraph clustering using a new Laplacian tensor with applications in image processing. SIAM J. Imaging Sci. **13**(3), 1157–1178 (2020)
9. De Lathauwer, L., De Moor, B.: From matrix to tensor: multilinear algebra and signal processing. In: Institute of Mathematics and its Applications Conference Series, vol. 67, pp. 1–16. Citeseer (1998)
10. Gandy, S., Recht, B., Yamada, I.: Tensor completion and low-n-rank tensor recovery via convex optimization. Inverse Prob. **27**(2), 025010 (2011)
11. Hao, N., Kilmer, M.E., Braman, K., Hoover, R.C.: Facial recognition using tensor-tensor decompositions. SIAM J. Imaging Sci. **6**(1), 437–463 (2013)
12. Hillar, C.J., Lim, L.H.: Most tensor problems are NP-hard. J. ACM **60**(6), 1–39 (2013)
13. Hu, W., Tao, D., Zhang, W., Xie, Y., Yang, Y.: The twist tensor nuclear norm for video completion. IEEE Trans. Neural Netw. Learn. Syst. **28**(12), 2961–2973 (2017)
14. Jiang, F., Liu, X.Y., Lu, H., Shen, R.: Anisotropic total variation regularized low-rank tensor completion based on tensor nuclear norm for color image inpainting. In: 2018 IEEE International Conference on Acoustics, Speech and Signal Processing (ICASSP). IEEE (2018)
15. Kasai, H.: Online low-rank tensor subspace tracking from incomplete data by CP decomposition using recursive least squares. In: 2016 IEEE International Conference on Acoustics, Speech and Signal Processing (ICASSP). IEEE (2016)
16. Kiers, H.A.L.: Towards a standardized notation and terminology in multiway analysis. J. Chemom. **14**(3), 105–122 (2000)
17. Kilmer, M.E., Braman, K., Hao, N., Hoover, R.C.: Third-order tensors as operators on matrices: a theoretical and computational framework with applications in imaging. SIAM J. Matrix Anal. Appl. **34**(1), 148–172 (2013)
18. Kilmer, M.E., Martin, C.D.: Factorization strategies for third-order tensors. Linear Algebra Appl. **435**(3), 641–658 (2011)
19. Kolda, T.G., Bader, B.W.: Tensor decompositions and applications. SIAM Rev. **51**(3), 455–500 (2009)
20. Kroonenberg, P.M.: Three-Mode Principal Component Analysis: Theory and Applications, vol. 2. DSWO Press, Leiden (1983)
21. Lathauwer, L.D., Vandewalle, J.: Dimensionality reduction in higher-order signal processing and rank-$(R_1, R_2, \ldots, R_N)$ reduction in multilinear algebra. Linear Algebra Appl. **391**, 31–55 (2004)
22. Li, S., Liu, Q.: Multi-filters guided low-rank tensor coding for image inpainting. In: 2017 2nd International Conference on Image, Vision and Computing (ICIVC). IEEE (2017)
23. Liu, J., Musialski, P., Wonka, P., Ye, J.: Tensor completion for estimating missing values in visual data. IEEE Trans. Pattern Anal. Mach. Intell. **35**(1), 208–220 (2013)
24. Liu, Y., Long, Z., Zhu, C.: Image completion using low tensor tree rank and total variation minimization. IEEE Trans. Multim. **21**(2), 338–350 (2019)

25. Liu, Y., Shang, F.: An efficient matrix factorization method for tensor completion. IEEE Signal Process. Lett. **20**(4), 307–310 (2013)
26. Long, Z., Liu, Y., Chen, L., Zhu, C.: Low rank tensor completion for multiway visual data. Signal Process. **155**, 301–316 (2019)
27. Lu, C., Feng, J., Chen, Y., Liu, W., Lin, Z., Yan, S.: Tensor robust principal component analysis: exact recovery of corrupted low-rank tensors via convex optimization. In: 2016 IEEE Conference on Computer Vision and Pattern Recognition (CVPR). IEEE (2016)
28. Martin, C.D., Shafer, R., LaRue, B.: An order-p tensor factorization with applications in imaging. SIAM J. Sci. Comput. **35**(1), A474–A490 (2013)
29. Martin, D., Fowlkes, C., Tal, D., Malik, J.: A database of human segmented natural images and its application to evaluating segmentation algorithms and measuring ecological statistics. In: Proceedings Eighth IEEE International Conference on Computer Vision (ICCV). IEEE (2001)
30. Mitchell, B.C., Burdick, D.S.: Slowly converging PARAFAC sequences: swamps and two-factor degeneracies. J. Chemom. **8**(2), 155–168 (1994)
31. Muti, D., Bourennane, S.: Multidimensional filtering based on a tensor approach. Signal Process. **85**(12), 2338–2353 (2005)
32. Roughan, M., Zhang, Y., Willinger, W., Qiu, L.: Spatio-temporal compressive sensing and internet traffic matrices (extended version). IEEE/ACM Trans. Netw. **20**(3), 662–676 (2012)
33. Tan, H., Wu, Y., Shen, B., Jin, P.J., Ran, B.: Short-term traffic prediction based on dynamic tensor completion. IEEE Trans. Intell. Transp. Syst. **17**(8), 2123–2133 (2016)
34. The abilene observatory data collections (2013). http://abilene.internet2.edu/observatory/data-collections.html
35. Tucker, L.R.: Some mathematical notes on three-mode factor analysis. Psychometrika **31**(3), 279–311 (1966)
36. Vasilescu, M.A.O., Terzopoulos, D.: Multilinear analysis of image ensembles: TensorFaces. In: Computer Vision-ECCV 2002, pp. 447–460. Springer, Berlin (2002)
37. Wang, Z., Bovik, A.C., Sheikh, H.R., Simoncelli, E.P.: Image quality assessment: from error visibility to structural similarity. IEEE Trans. Image Process. **13**(4), 600–612 (2004)
38. Wen, Z., Yin, W., Zhang, Y.: Solving a low-rank factorization model for matrix completion by a nonlinear successive over-relaxation algorithm. Math. Program. Comput. **4**(4), 333–361 (2012)
39. Xu, Y.: Alternating proximal gradient method for sparse nonnegative Tucker decomposition. Math. Program. Comput. **7**(1), 39–70 (2015)
40. Xu, Y., Hao, R., Yin, W., Su, Z.: Parallel matrix factorization for low-rank tensor completion. Inverse Probl. Imaging **9**(2), 601–624 (2015)
41. Xu, Y., Yin, W.: A block coordinate descent method for regularized multiconvex optimization with applications to nonnegative tensor factorization and completion. SIAM J. Imaging Sci. **6**(3), 1758–1789 (2013)
42. Yu, Q., Zhang, X., Chen, Y., Qi, L.: Low Tucker rank tensor completion using a symmetric block coordinate descent method. Numer. Linear Algebra Appl. **30**, e2464 (2022)
43. Zhang, L., Zhang, L., Mou, X., Zhang, D.: FSIM: a feature similarity index for image quality assessment. IEEE Trans. Image Process. **20**(8), 2378–2386 (2011)
44. Zhang, X., Ng, M.K.: A corrected tensor nuclear norm minimization method for noisy low-rank tensor completion. SIAM J. Imaging Sci. **12**(2), 1231–1273 (2019)
45. Zhang, Z., Ely, G., Aeron, S., Hao, N., Kilmer, M.: Novel methods for multilinear data completion and de-noising based on tensor-SVD. In: 2014 IEEE Conference on Computer Vision and Pattern Recognition. IEEE (2014)
46. Zheng, Y.B., Huang, T.Z., Zhao, X.L., Jiang, T.X., Ma, T.H., Ji, T.Y.: Mixed noise removal in hyperspectral image via low-fibered-rank regularization. IEEE Trans. Geosci. Remote Sens. **58**(1), 734–749 (2020)
47. Zhou, H., Zhang, D., Xie, K., Chen, Y.: Spatio-temporal tensor completion for imputing missing internet traffic data. In: 2015 IEEE 34th International Performance Computing and Communications Conference (IPCCC). IEEE (2015)
48. Zhou, P., Lu, C., Lin, Z., Zhang, C.: Tensor factorization for low-rank tensor completion. IEEE Trans. Image Process. **27**(3), 1152–1163 (2018)